Protection of Regulatory T Cells from Fragility and Inactivation in the Tumor Microenvironment

Hongru Zhang[1], Vivek S. Tomar[1], Jinyang Li[2], Raghavendra Basavaraja[1], Fangxue Yan[1], Jun Gui[1], Noreen McBrearty[1], Tara Lee Costich[3], Daniel P. Beiting[4], M. Andres Blanco[1], Jose R. Conejo-Garcia[3], Gurpanna Saggu[5], Allison Berger[5], Yulia Nefedova[6], Dmitry I. Gabrilovich[7], and Serge Y. Fuchs[1]

ABSTRACT

Fragility of regulatory T (Treg) cells manifested by the loss of neuropilin-1 (NRP1) and expression of IFNγ undermines the immune suppressive functions of Treg cells and contributes to the success of immune therapies against cancers. Intratumoral Treg cells somehow avoid fragility; however, the mechanisms by which Treg cells are protected from fragility in the tumor microenvironment are not well understood. Here, we demonstrate that the IFNAR1 chain of the type I IFN (IFN1) receptor was downregulated on intratumoral Treg cells. Downregulation of IFNAR1 mediated by p38α kinase protected Treg cells from fragility and maintained NRP1 levels, which were decreased in response to IFN1. Genetic or pharmacologic inactivation of p38α and stabilization of IFNAR1 in Treg cells induced fragility and inhibited their immune suppressive and protumorigenic activities. The inhibitor of sumoylation TAK981 (Subasumstat) upregulated IFNAR1, eliciting Treg fragility and inhibiting tumor growth in an IFNAR1-dependent manner. These findings describe a mechanism by which intratumoral Treg cells retain immunosuppressive activities and suggest therapeutic approaches for inducing Treg fragility and increasing the efficacy of immunotherapies.

Introduction

Immune-privileged niches in the tumor microenvironment undermine antitumor immunity and limit the efficacy of immune therapies (1, 2). Regulatory T (Treg) cells are an important cellular component of the intratumoral immune suppressive milieu that promotes the growth and progression of solid tumors (3–5). Treg cells are immunosuppressive $CD4^+$ T cells that express forkhead box P3 (FOXP3, a.k.a. scurfin) and play a key role in restricting the activity of the immune system and preventing autoimmune disorders (6, 7).

The protumorigenic effects of Treg cells are bolstered by their accumulation inside tumors and further augmented by stress stimuli in the tumor microenvironment (8). The presence and immune suppressive activities of Treg cells in the tumor microenvironment are often associated with poor prognosis in patients with cancer (9–11). The immunomodulatory functions of Treg cells are tempered by inflammatory stimuli (3, 4). Although such stimuli are abundant in the tumor microenvironment, intratumoral Treg cells maintain their suppressive activities. Mechanisms protecting Treg cells from inactivation in the tumor microenvironment are yet to be understood.

The importance of Treg cells in tumor growth and escape from immune surveillance is highlighted by the discovery that the efficacy of immune checkpoint therapy depends on the presence of specific dysfunctional IFNγ-expressing Treg cells termed fragile Treg cells (12, 13). The state of fragility involves expression of IFNγ and attenuation of immune suppressive activities without loss of FOXP3 (13), which is often characteristic of other types of destabilization and plastic metamorphoses of Treg cells (14). Treg-cell fragility is triggered by ablation of neuropilin-1 (NRP1) and ensuing cytoplasmic retention and inactivation of the transcription factor FOXO3a (15).

NRP1 is a type 1 transmembrane protein, which functions as a coreceptor that supports signaling by TGFβ and VEGF (16). NRP1 plays a critical role in the stability and function of Treg cells (15, 17). It acts to guide Treg cells into the tumor in response to tumor-derived VEGF (18). Expression of NRP1 on Treg cells is important to support tumor growth (12, 18). The current paradigm indicates that targeting the key actors that regulate Treg-cell fragility should open novel avenues for anticancer treatment and improve the efficacy of existing immune therapies (13, 19).

The mechanisms by which the tumor microenvironment can circumvent fragility and preserve the immune suppressive properties of Treg cells remain to be fully understood. The data presented here implicate p38α kinase–driven inactivation of the IFNAR1 chain for the type I IFN (IFN1) receptor in the regulation of Treg-cell fragility and protumorigenic functions. Cell surface levels of IFNAR1, which plays a key role in all cell responses to IFN1 (20), are regulated by phosphorylation-dependent ubiquitination and subsequent degradation (21). This process is accelerated by tumor-derived factors and the stressful conditions of the tumor microenvironment (22–24). Downregulation of IFNAR1 on intratumoral $CD8^+$ CTL contributes to formation of immune-privileged niches by depriving CTL of the prosurvival effects of IFN1 (25).

The data presented here suggest that p38α-driven downregulation of IFNAR1 on intratumoral or *in vitro*–induced Treg cells preserves their abilities to express NRP1, to suppress the expression of IFNγ, and to elicit their immune suppressive activities *in vitro* and *in vivo*. Consistent with this, knockout of p38α in Treg cells inactivated their immune suppressive function and inhibited tumor growth in an IFNAR1-dependent manner. Furthermore, small-molecule agents

[1]Department of Biomedical Sciences, School of Veterinary Medicine, University of Pennsylvania, Philadelphia, Pennsylvania. [2]Department of Pathology and Laboratory Medicine, Perelman School of Medicine, University of Pennsylvania, Philadelphia, Pennsylvania. [3]Department of Immunology, H. Lee Moffitt Cancer Center and Research Institute, Tampa, Florida. [4]Department of Pathobiology, School of Veterinary Medicine, University of Pennsylvania, Philadelphia, Pennsylvania. [5]Takeda Development Center Americas, Inc., Lexington, Massachusetts. [6]The Wistar Institute, Philadelphia, Pennsylvania. [7]AstraZeneca, Gaithersburg, Maryland.

Corresponding Author: Serge Y. Fuchs, University of Pennsylvania, 380 S. University Ave, Philadelphia, PA 19104. Phone: 215-573-6949; E-mail: syfuchs@upenn.edu

Cancer Immunol Res 2022;10:1490–505

doi: 10.1158/2326-6066.CIR-22-0295

that maintain IFNAR1 levels (such as inhibitors of p38 kinase or of protein sumoylation) induced Treg fragility and restricted tumor growth.

Materials and Methods

Study approvals

Human peripheral blood mononuclear cells (PBMC) were collected from 15 patients diagnosed with different types of cancers, including colon cancer (1), melanoma (1), diffuse large B-cell lymphoma (1), gastrointestinal stroma tumor (1), granulosa cell tumor (1), lung metastatic adenocarcinoma (1), ovarian cancer (4), endometriosis (2), and benign mass (3). There were no exclusion criteria for these patients. These cells were collected under informed written consent and then the samples were deidentified so they could not be directly or indirectly linked to individual patients. Studies involving collection and use of these cells adhered to the U.S. Common rule and were also compliant with the declaration of Helsinki and the Belmont report. These studies were done under protocols approved by the Committee for the Protection of Human Subjects at H. Lee Moffitt Cancer Center (Institutional Review Board protocols MCC#19767 and MCC#18974).

All animal experiments were approved by the Institutional Animal Care and Use Committee (IACUC) of the University of Pennsylvania (Philadelphia, PA) and were carried out in accordance with the IACUC guidelines.

Animal studies

All mice had water *ad libitum* and were fed regular chow. Mice were maintained in a specific-pathogen-free facility in accordance with American Association for Laboratory Animal Science guidelines. Mice were housed in single-sex cages at 20°C ± 2°C under a 12-hour light/12-hour dark photoperiod with the lights on at 7:00 A.M. C57BL/6 littermate *Ifnar1*$^{+/+}$ ("WT") and *Ifnar1*^{S526A} mice (SA) were described previously (26); Balb/c wild-type (WT) and SA mice were obtained after 10 crosses of C57BL/6 mice into WT Balb/c animals (Jackson Labs, stock no. 000651). The OT-I mice used to generate OT-I CTLs were obtained from Jackson Labs (C57BL/6-Tg(TcraTcrb)1100Mjb/J, stock no. 003831). Rag1-null mice were also from Jackson Lab (B6.129S7-Rag1tm1Mom/J, stock no. 002216). The SA mice were donated to Jackson Labs and are available from this source (*C57BL/6-Ifnar1tm1.1Syfu/J*; stock no. 035564). *Ifnar1*$^{f/f}$ mice (*B6(Cg)-Ifnar1tm1.1Ees/J*, stock no. 028256) and *B6.129(Cg)-Foxp3*$^{tm4(YFP/icre)Ayr}$*/J (Foxp3-Cre*, stock no. 016959) mice were purchased from Jackson Laboratory. *Foxp3-Cre* mice were crossed with *Ifnar1*$^{f/f}$ mice or *Mapk14*$^{f/f}$ mice (gift from Yibin Wang, UCLA) to generate *Foxp3-cre::Ifnar1*$^{f/f}$ mice, *Foxp3-cre::Mapk14*$^{f/f}$, or *Foxp3-cre::Mapk14*$^{f/f}$*Ifnar1*$^{f/f}$ mice litter-mates. *Foxp3-Cre* mice were also crossed with SA mice for obtaining YFP^{+} SA Treg cells. All these mice were viable and fertile with no reported abnormalities. The genotyping PCR primers are provided in Supplementary Table S1. Littermate animals approximately 8 weeks old of both sexes from different cages were randomly assigned into the experimental groups. These randomized experimental cohorts were either cohoused or systematically exposed to the bedding of other groups to ensure equal exposure to the microbiota of all groups.

Cell lines

Mouse cell lines MC38, B16F10, CT26, and EL4 were purchased from ATCC between 2016 and 2019, routinely tested for *Mycoplasma*, and maintained according to ATCC recommendations. The mouse MC38OVA cell line was generously provided by Dr. Suzanne Ostrand-Rosenberg (University of Maryland, Baltimore, MD) in 2015. MC38OVA cells were further engineered to stably express Firefly luciferase, as described previously (27). These cell lines have not been reauthenticated. All cells were cultured at 37°C with 5% CO_2 in DMEM (Gibco, catalog no. 11965-084) supplemented with 10% heat-inactivated FBS (Hyclone, catalog no. SH30071.03), 100 U/mL penicillin-streptomycin (Thermo Fisher Scientific, catalog no. 15140122), and L-glutamine (Gibco, catalog no. 25030081). Only cells that were continually cultured for less than 4 weeks were used in the experiments.

Tumor models

MC38, B16F10, and CT26 cells were injected in 100 μL of serum-free media subcutaneously into the right flank of the indicated syngeneic mice; the number of cells injected is indicated in specific figure legends. Tumor volumes were measured using calipers three times per week starting at day 7 after inoculation. The maximal tumor size allowed was 1,000 mm^3 and the maximal tumor size was not exceeded.

RNA sequencing analysis

WT and SA Treg cells were differentiated *in vitro* according to the protocol below (see Generation of iTreg cells). Total RNA was isolated from the Treg cells (1×10^6 cells per group) using an miRNeasy mini kit (QIAGEN, catalog no. 74004). These samples were run using Takara Clontech's SMART Seq HT Kit (catalog no. 634470) to make cDNA. Libraries were then generated using Illumina's Nextera kit (catalog no. SKU301067). In this kit, rRNA depletion is done using Takara's SMART technology to perform positive selection of mRNA; in other words, the SMART system enriches only mRNA. Data were collected with Illumina BeadStudio 3.1.1.0 software, and statistical analyses were conducted on the IlluminaGUI R-package. Raw fastq files were used as input files for transcript quantification with Salmon. Reference genome mm10 was used for normalization. Differential gene expression analysis was done using DESeq2. Gene set enrichment analysis (GSEA) was done using the prerank mode and gene list was ranked by the stat value from DESeq2 analysis. The data can be found in Gene Expression Omnibus (GEO accession GSE182029).

Single-cell RNA sequencing analysis

Immune cells (CD45^{+}CD3^{+}) were isolated from MC38 tumors growing in WT or SA mice on day 14 after inoculation of 1×10^6 cells/mouse. $N = 9{,}725$ cells were used for the single-cell RNA (scRNA-seq) analyses. Cells were run through 10X Genomics' Chromium Next GEM Single Cell 3′ Reagent Kit v3.1 with single indexes. Library preparation was also done with 10X Genomics' Chromium Next GEM Single Cell 3′ Reagent Kit v3.1 (single index). It was quantified using Tapestation 4200 and Qubit 3. There were no custom adaptors. We used a 150 cycle High Output kit with version chemistry 2.5. This would have gotten you 400 million reads and 200 million read pairs per sample. It was sequenced as paired end: 28 bp by 91 bp with a single 8 bp index. scRNA-seq libraries were prepared following the protocol from 10X Genomics and then sequenced using an Illumina Nextseq 550. BCL files were generated for further analysis. Alignment, filtering, barcode counting, and unique molecular identifier counting were performed using Cell Ranger v.4.0.0 (https://support.10xgenomics.com/single-cell-gene-expression/software/overview/welcome). Data were further analyzed using Seurat v.3.1.5 (https://satijalab.org/seurat/). Cells with at least 500 detected genes, at least 1,000 detected RNA, and no more than 50,000 RNA were included in downstream analyses. Raw unique molecular identifier counts were normalized to

unique molecular identifier count per million total counts and log transformed, using NormalizeData function. Reference genome mm10 was used for normalization. Data were scaled with regression to nCount RNA and group (WT vs. SA), using ScaleData function. Variable genes were selected on the basis of average expression and dispersion. Principal component analysis was performed with default settings. Clusters and t-distributed stochastic neighbor embedding (t-SNE) plots were generated based on selected principal component analysis dimensions. t-SNE plots and dot plots showing the expression of labeled genes were performed using FeaturePlot and DotPlot functions. Differential gene expression analysis was performed using FindMarkers function with following parameters: min.cells.group = 1, min.cells.feature = 1, min.pct = 0, logfc.threshold = 0, only.pos = FALSE. Resulted output (ave_logFC) was utilized as input for GSEA with prerank mode. When we analyze the Treg function, we used the following previously published gene signatures: Treg effector gene signature: GSE14415; Treg dysfunction gene signature: GSE42021. The data can be found in GEO (accession no. 171055).

Flow cytometry analysis

Tumors or spleens were incubated in dissociation solution (RPMI1640 without FBS) with 2 mg/mL Collagenase II (MP Biomedicals, catalog no. MP21005025), or 1 mg/mL Collagenase IV (Sigma, catalog no. 11088882001) plus 100 μg/mL DNase I (Roche, catalog no. 10104159001) for 1 hour at room temperature with continuous agitation. Cells were filtered through a 70 μmol/L cell strainer and resuspended in PBS with 1% BSA, 1 mmol/L Ethylenediaminetetraacetic acid. The isolated cells were incubated with anti-mouse CD16/CD32 (BioLegend, Clone 93 catalog no. 101302, 1:50) for 15 minutes on ice to block nonspecific Fc receptor binding. Cells were then stained with antibodies specific for cell surface markers for 30 minutes on ice. For intracellular staining, cells were stimulated with phorbol 12-myristate 13-acetate (PMA; Sigma, P8139-1 mg), ionomycin (Sigma, i9657-1 mg), and Golgi-stop (BD, 550583) for 6 hours as described elsewhere (27), then the cells were stained according to recommendations of the manufacturer of the eBioscience Foxp3/Transcription Factor Staining Buffer Set (catalog no. 00-5523-00). The antibodies used for flow cytometry are listed in Supplementary Table S2. The samples were acquired by LSRFortessa flow cytometry (BD Biosciences). Data were analyzed with FlowJo software (FlowJo 9.9.6 or FlowJo 10). The cell surface levels of analyzed proteins are shown as difference between actual value minus isotype control [Δmean fluorescence intensity (MFI)].

Human PBMC samples were first stained with antibodies specific for cell surface markers for 30 minutes on ice. For intracellular staining, cells were directly stained according to recommendations of the manufacturer of the eBioscience Foxp3/Transcription Factor Staining Buffer Set (catalog no. 00-5523-00) without stimulation.

OT-I cells intracellular staining

To measure the cytokines and/or effector molecules of the OT1 cells after coculture, cells were stimulated with PMA, ionomycin, and Golgi-stop for 6 hours, then the cells were stained according to recommendations of the manufacturer of the eBioscience Foxp3/Transcription Factor Staining Buffer Set (catalog no. 00-5523-00).

qPCR

Total RNA was extracted from WT and SA *in vitro* differentiated Treg (iTregs) using TRIzol reagent (Invitrogen, catalog no. 15596026). The High-Capacity RNA-to-cDNA Kit (Applied Biosystems, catalog no. 4387406) was used to make complementary DNA. Real-time PCR was performed using SYBR Green Master Mix reagents (Applied Biosystems, catalog no. 4309155). The expression of each gene was calculated on the basis of the cycle threshold, set within the linear range of DNA amplification. The relative expression was calculated by the cycle threshold method ($2^{-\Delta CT}$), with normalization of raw data to a housekeeping gene (β-Actin). The samples were run by applied biosystems ViiA 7. The primer sequences of the genes detected and for normalization are provided in Supplementary Table S3.

Cytotoxicity assays

The ability of OT-I cells to kill target MC38OVA cells expressing luciferase was evaluated in a luciferase-based cytotoxicity assay as described previously (27). Briefly, target MC38OVA cells were cocultured with CTL at the indicated E:T ratios in 96-well black plates at a total volume of 200 μL. Target cells alone were seeded in parallel at the same density to quantify the spontaneous death luciferase expression (relative luminescent units; spontaneous death RLU). Target cells lysed with water were considered as the maximal killing (maximal killing RLU). Following coculture, 100 μL of luciferase substrate (Bright-Glo; Promega, catalog no. E6110) was added to the remaining supernatant and cells. In IFNγ pretreatment experiments, WT iTregs were pretreated with or without mIFNβ (1,000 IU/mL, BioLegend, catalog no. 575302) for 24 hours before coculture with the OT-I cells. Luminescence was measured after a 10-minute incubation using the EnVision (PerkinElmer) plate reader. The percent cell lysis was obtained using the following calculation: % lysis = 100× (spontaneous death RLU − test RLU)/(spontaneous death RLU − maximal killing RLU).

Generation of iTreg cells

Mouse iTreg cells were differentiated from naive $CD4^+$ T cells using the commercial CellXVivo Treg-cell differentiation kit (CDK007, R&D). Briefly, naïve $CD4^+$ T cells were isolated from mouse spleens using the EasySep Mouse Naïve $CD4^+$ T Cell Isolation Kit (Stemcell, 19765) and activated by plate coated anti-CD3 (10 μg/mL, BioLegend, 100340) and anti-CD28 (2 μg/mL, BioLegend, 102116) in the presence of TGFβ (10 ng/mL, R&D, 7666-MB-005/CF) and IL2 (2 ng/mL, BioLegend, 575402) for 5–7 days. The yield and purity of Treg fraction was monitored by analysis of $CD4^+Foxp3^+$ cells using flow cytometry.

Ex vivo immunosuppression assays

Treg cells were either *in vitro* differentiated or isolated from MC38 tumors grown in WT or SA mice using a MACS separation kit (Miltenyi Biotec, catalog no. 130-091-041) according to the manufacturer's instructions. iTreg cells were not restimulated before being used either in cytotoxicity assays or in T-cell proliferation assays. For the cytotoxicity assay (described above), Treg or iTreg cells were cocultured with OT-I cells (1:3 or at indicated conditions) followed by assessment of killing MC38OVA cells as described above. For T-cell proliferation assays, splenic naïve $CD8^+$ T cells were isolated from WT mice using a kit (Stemcell, catalog no. 19858), labeled with CellTrace Violet (Thermo Fisher Scientific, catalog no. C34557), and cultured either alone or with the indicated Treg cells (Treg: T = 1:3) in the presence of magnetic beads precoated with agonist antibodies against CD3 and CD28 (Gibco, catalog no. 11453D), and proliferation was measured by flow cytometry after 3 days. Proliferation Index is the total number of divisions divided by the number of cells that went into division, which were analyzed by FlowJo 10.

Drug treatment

The p38 kinase inhibitor ralimetinib (LY2228820, LY, Selleckcem, S1494) was dissolved in 1% methylcellulose and administered by oral gavage according to the experiment design at the dose of 10 mg/kg

body weight. The sumoylation inhibitor TAK981 (produced by Takeda Development Center Americas, Inc.) was dissolved in 40% HPBCD, 5% 1N HCl, and 4.5% NaOH and administered by intravenous injection according to the experiment design at the dose of 15 mg/kg body weight, as described previously (28).

Cell sorting

To obtain the Treg cells (YFP^+) from MC38 tumor-bearing Foxp3Cre mice (WT and SA), we used FACS to select the YFP^+ cells to be next used for the *in vitro* coculture experiment.

Cell adoptive transfer

MC38OVA tumor cells (1×10^6) were subcutaneously injected into $Rag1^{-/-}$ mice. The iTreg (WT or SA, 2.5×10^6/mouse) were adoptively transferred intravenously into MC38OVA tumor–bearing mice at day 11 after tumor inoculation. Then 1 day later, the OT-I cells (5×10^6/mouse) were adoptively transferred intravenously.

Microscopy

WT and SA iTreg were induced according to the protocol described above. Then FOXO3a staining was performed on iTregs without stimulation. Briefly, cells were harvested, fixed in 1% paraformaldehyde in PBS (room temperature 30 minutes), and permeabilized with 0.1% Triton X-100 in TBS (ambient temperature, 20 minutes). After blocking with 5% BSA (room temperature 1 hour), cells were stained with anti-Foxo3a (Cell Signaling Technology, 2497) overnight in Tris-buffered 1% BSA. After several washes, cells were stained with Alexa Fluor 647–conjugated anti-rabbit IgG (Invitrogen, A32733, 1:500), and sytox Green (Thermo Fisher Scientific, S7020, 1:10,000) and then washed several times. Then cells were resuspended in Fluoromount G medium (Southern Biotech: 0100-01) and put into the slides. Then the slides were checked by the confocal microscopy. The nuclear and cytoplasmic volumes of Foxo3a fluorescence of 20–30 stacks were calculated using Slidebook (3i, Inc.) software in arbitrary fluorescence units and analyzed in Graphpad Prism.

NRP1 overexpression

We subcloned mouse NRP1 from pCherry-mNrp1 (Addgene, catalog no. 21934) into the cloning site of the lentivirus vector pCDH-EF1-FHC (Addgene, catalog no. 64874) and then produced lentivirus using the packaging plasmids psPAX2 (Addgene, catalog no. 12260), and pMD2.G (catalog no. 12259). Then SA iTreg were infected by the NRP1 lentivirus, and the function of these iTreg was detected by performing the cytotoxicity assay.

TAK981 cell treatment

WT iTreg were induced *in vitro* and then treated with or without TAK981 (100 nmol/L in DMSO) for 24 hours. After treatment, IFNAR1, IFNγ, and NRP1 levels were checked by the flow cytometry.

IFNβ cell treatment

iTreg or EL4 cells were treated with or without mIFNβ (1,000 IU/mL) for the indicated time. Then NRP1 mRNA or protein levels were determined by qPCR and flow cytometry, respectively.

Statistical analysis and reproducibility

All described results are representative of at least three independent experiments. Statistical analyses and the number of samples (n) are described in detail in the legend for each figure panel. No statistical method was used to predetermine sample size. Data were presented as average ± SEM. Statistical analysis was performed using Microsoft Excel (Microsoft) or GraphPad Prism 8 software (GraphPad). Two-tailed unpaired Student t test was used for the comparison between two groups. One-way ANOVA or two-way ANOVA followed by the Sidak or Tukey test was used for the multiple comparisons. Repeated-measures two-way ANOVA (mixed model) followed by the Sidak multiple comparisons test was used for analysis of the tumor growth curve. The Kaplan–Meier curves were used to depict the survival for mice; the log-rank test or Gehan–Breslow–Wilcoxon test was used to analyze the differences between the groups. Fisher test was used for other comparisons. A value of $P < 0.05$ was considered significant. Henceforth asterisks: *, $P < 0.05$; **, $P < 0.01$; ***, $P < 0.001$; ****, $P < 0.0001$; ns, not significant. The experiments were not randomized, except that the mice were randomly grouped before treatment.

Data availability

The scRNA-seq data and the microarray data generated in this study are publicly available in GEO at GSE171055 and GSE182029, respectively. All other data are available within the article and its Supplementary Data or from the corresponding author upon reasonable request.

Results

IFNAR1 downregulation enables the immune suppressive and protumorigenic activities of Treg cells

Phosphorylation-driven ubiquitination, downregulation, and degradation of IFNAR1 protein in WT cells in response to inflammation, tumor-derived factors, and tumor microenvironment stress inhibits the IFN1 pathway (22–24, 26). The biological significance of IFNAR1 downregulation is evident from studies in the $Ifnar1^{S526A}$ knock-in mice (henceforth, termed "SA"). Cells of these mice express the SA mutant version of IFNAR1, which is deficient in phosphorylation-dependent downregulation in response to inflammation, tumor-derived factors, or stress (22–24, 26). SA mice maintain IFNAR1 levels even under inflammatory conditions (29). Although these mice develop normally and, when unchallenged, do not display any overt phenotypes (29), it has been reported that development and growth of tumors are inhibited in SA mice (25, 30).

The antitumorigenesis phenotype in SA mice has been largely attributed to stabilization of IFNAR1 in intratumoral CTL. Endogenous and chimeric antigen receptor–bearing SA $CD8^+$ T cells exhibit greater viability and antitumor activities compared with their WT counterparts (25, 27). However, it is not well understood why the antitumor activities of these SA CTL are not restrained by Treg cells. Thus, we sought to characterize the status of Treg cells in SA mice.

We first compared characteristics of Treg cells from naïve WT and SA mice (Supplementary Fig. S1A). Splenocytes from SA mice displayed higher levels of IFNAR1 but similar frequencies of $CD4^+$, $CD8^+$ and Treg cells (Supplementary Fig. S1B). Splenic WT and SA Treg cells displayed comparable protein levels of Foxp3, Helios, Tbet, Eos, CTLA4, CD40 L, and IL17 (Supplementary Fig. S1C). As expected, splenic Tregs from SA mice express higher levels of cell surface IFNAR1 compared with their WT counterparts. Intriguingly, we also noted an increase in the intracellular levels of IFNγ and IL2 in SA Treg cells (Supplementary Fig. S1C).

Growth of MC38 or CT26 colon adenocarcinomas and of B16F10 melanoma tumors was significantly decelerated in SA mice (**Fig. 1A–D**; Supplementary Fig. S1D and S1E; ref. 25). Analysis of cell surface levels of IFNAR1 revealed its downregulation on the intratumoral Treg cells in WT mice compared with splenic Treg cells, but no such downregulation was observed on the intratumoral Treg

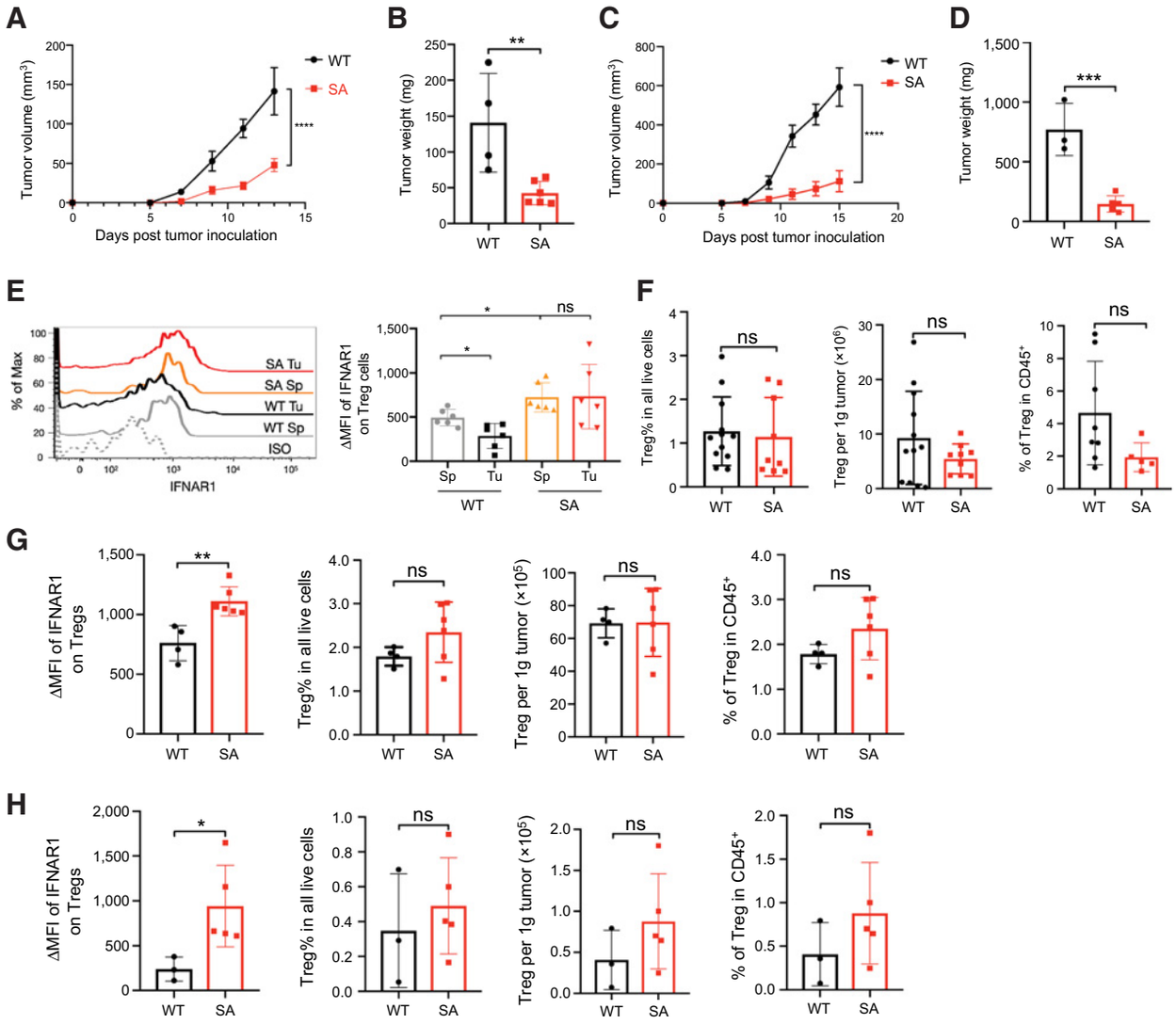

Figure 1.

IFNAR1 is downregulated on intratumoral Treg cells. **A,** Growth of CT26 tumors developing after 1×10^6 CT26 cells were injected subcutaneously into BALB/c WT and SA mice. Tumor volumes were measured three times per week. Data are shown as mean ± SEM ($n = 4$–6 mice). Statistical analysis was performed using two-way ANOVA with Tukey multiple comparisons test. ****, $P < 0.0001$. **B,** Weight of CT26 tumors grown in mice of indicated genotypes on day 13 after inoculation. Data are shown as mean ± SEM ($n = 4$–6 mice). Two-tailed unpaired *t* test was performed for the comparisons between groups. **, $P = 0.0088$. **C,** Growth of B16F10 tumors developing after 1×10^6 B16F10 cells were injected after subcutaneous into C57BL/6 WT and SA mice. Tumor volumes were measured three times per week. Data are shown as mean ± SEM ($n = 4$–6 mice). Statistical analysis was performed using two-way ANOVA with Tukey multiple comparisons test. ****, $P < 0.0001$. **D,** Weight of B16F10 tumors grown in mice of indicated genotypes on day 15 after inoculation. Data are shown as mean ± SEM ($n = 3$–5 mice). Two-tailed unpaired *t* test was performed for the comparisons between groups. ***, $P = 0.0008$. **E,** Flow cytometry analysis of levels of IFNAR1 on Treg cells ($CD45^+CD3^+CD4^+Foxp3^+$) in spleen (Sp) and tumor (Tu) tissues from WT or SA mice on day 21 after inoculation of subcutaneous MC38 tumors (1×10^6 cells/mouse). Quantification of the mean MFI is shown on the right ($n = 6$–8 mice). Statistical analysis was performed using ordinary one-way ANOVA with Tukey multiple comparisons test. *, $P < 0.05$. **F,** Frequencies and numbers of Treg cells in MC38 tumors grown in WT or SA mice on day 21 after inoculation. Data are shown as mean ± SEM ($n = 8$–11 mice). Two-tailed unpaired *t* test was performed for the comparisons between groups. **G,** IFNAR1 levels and frequencies and numbers of Treg cells in CT26 tumors grown in WT or SA mice on day 13 after inoculation. Data are shown as mean ± SEM ($n = 4$–6 mice). Two-tailed unpaired *t* test was performed for the comparisons between groups. **, $P = 0.0034$. **H,** IFNAR1 levels and frequencies and numbers of Treg cells in B16F10 tumors grown in WT or SA mice on day 15 after inoculation. Data are shown as mean ± SEM ($n = 3$–5 mice). Two-tailed unpaired *t* test was performed for the comparisons between groups. *, $P = 0.0439$.

cells in SA mice (**Fig. 1E**). Intratumoral SA Treg cells exhibited greater levels of IFNAR1 compared with intratumoral WT Tregs in all tumor models studied (**Fig. 1E**; Supplementary Fig. S1F and S1G). Numbers of intratumoral WT and SA Treg cells were comparable for MC38 (**Fig. 1F**; Supplementary Fig. S1H), CT26 (**Fig. 1G**), or B16F10 (**Fig. 1H**) tumors. These data suggest that downregulation of IFNAR1 does not affect recruitment and accumulation of Treg cells inside tumors.

We next focused on assessment of the regulatory activities of SA Treg cells. Regulatory functions are associated with expression of

checkpoint molecules (such as CTLA4 and LAG3), immune suppressive cytokines (such as TGFβ and IL10), and CD39 and CD73 ectonucleotidases, which are important for production of adenosine (reviewed in refs. 3–5). Adenosine produced by Treg cells stressed in the tumor microenvironment plays an important role in their regulatory activities (8). We found lower levels of CD73 on the cell surface of Treg cells isolated from MC38 tumors grown in SA mice compared with those from MC38 tumors grown in WT mice (**Fig. 2A**). We performed single-cell gene-expression profiling of T cells from these MC38 tumors (**Fig. 2B**) and focused our analysis on Treg cells. The expression profile from SA Treg cells (compared with WT) was notably enriched in IFNα response signatures (**Fig. 2C**) indicating that the IFN1 pathway is inhibited in WT Treg cells in the tumor microenvironment.

Additional analyses of genes associated with immune suppressive function showed that Treg cells isolated from tumors growing in SA mice expressed lower levels of *Ctla4*, *Tgfb1*, and *Ebi3* but not *Il10* or *Lag3* (**Fig. 2D**). SA Treg cells with elevated IFNAR1 levels also showed a decreased Treg effector signature and augmented Treg dysfunctional signature (**Fig. 2E**), suggesting that downregulation of IFNAR1 in WT Treg cells may plausibly help to protect them from dysfunction.

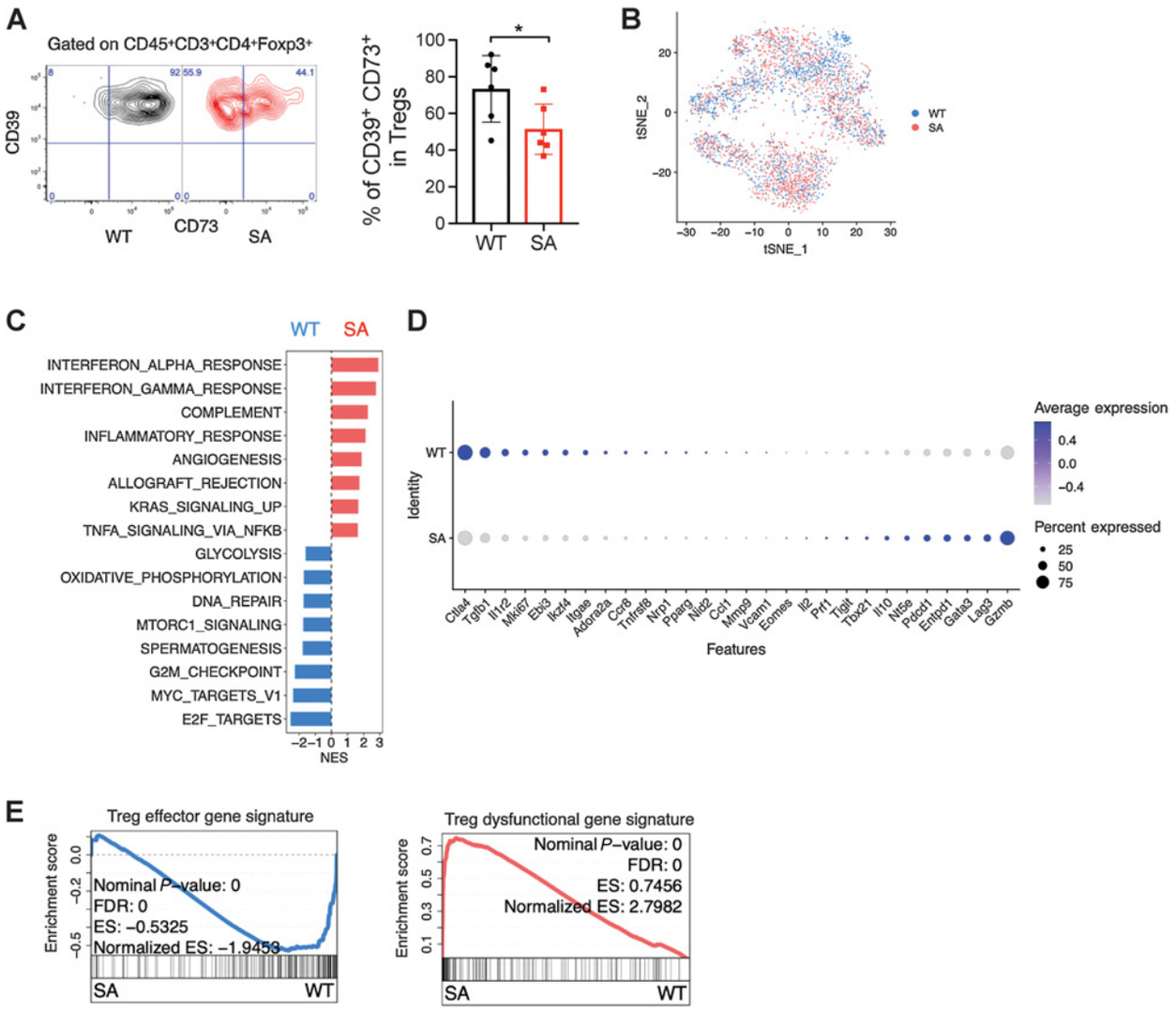

Figure 2.

Downregulation of IFNAR1 in Treg cells is associated with expression of immune suppressive mediators. **A,** Flow cytometry analysis of percentage of $CD73^+CD39^+$ Treg cells ($CD45^+CD3^+CD4^+Foxp3^+$) in tumors from WT and SA mice on day 21 after subcutaneous inoculation of 1×10^6 cells MC38 cells/mouse. Quantification data (on the right) are shown as mean ± SEM ($n = 6$ mice). Two-tailed unpaired *t* test was performed for the comparisons between groups. *, $P = 0.0395$. **B,** Immune cells ($CD45^+CD3^+$) were isolated from MC38 tumors growing in WT or SA mice on day 14 after inoculation of 1×10^6 cells/mouse. $N = 9{,}725$ cells were used for the scRNA-seq analyses. t-SNE plot of $CD3^+$ T cells with clusters demarcated by colors demonstrating WT (blue, $n = 2{,}075$ cells) and SA (red, $n = 2{,}038$ cells). **C,** GSEA of differentially expressed genes comparing Treg cells in WT and SA groups from B. Blue and red colors denote gene sets enriched in WT and SA, respectively. **D,** Dot plot showing the expression of immune suppressive function–related genes in Treg cells described in **B**. The size of the dot corresponds to the percentage of cells expressing the gene in each group and the color represents the average expression level. **E,** Leading-edge plots showing results from GSEA of Treg cell function-relevant signatures in Treg cells described in **B**. (Treg effector gene signature: GSE14415; Treg dysfunction gene signature: GSE42021).

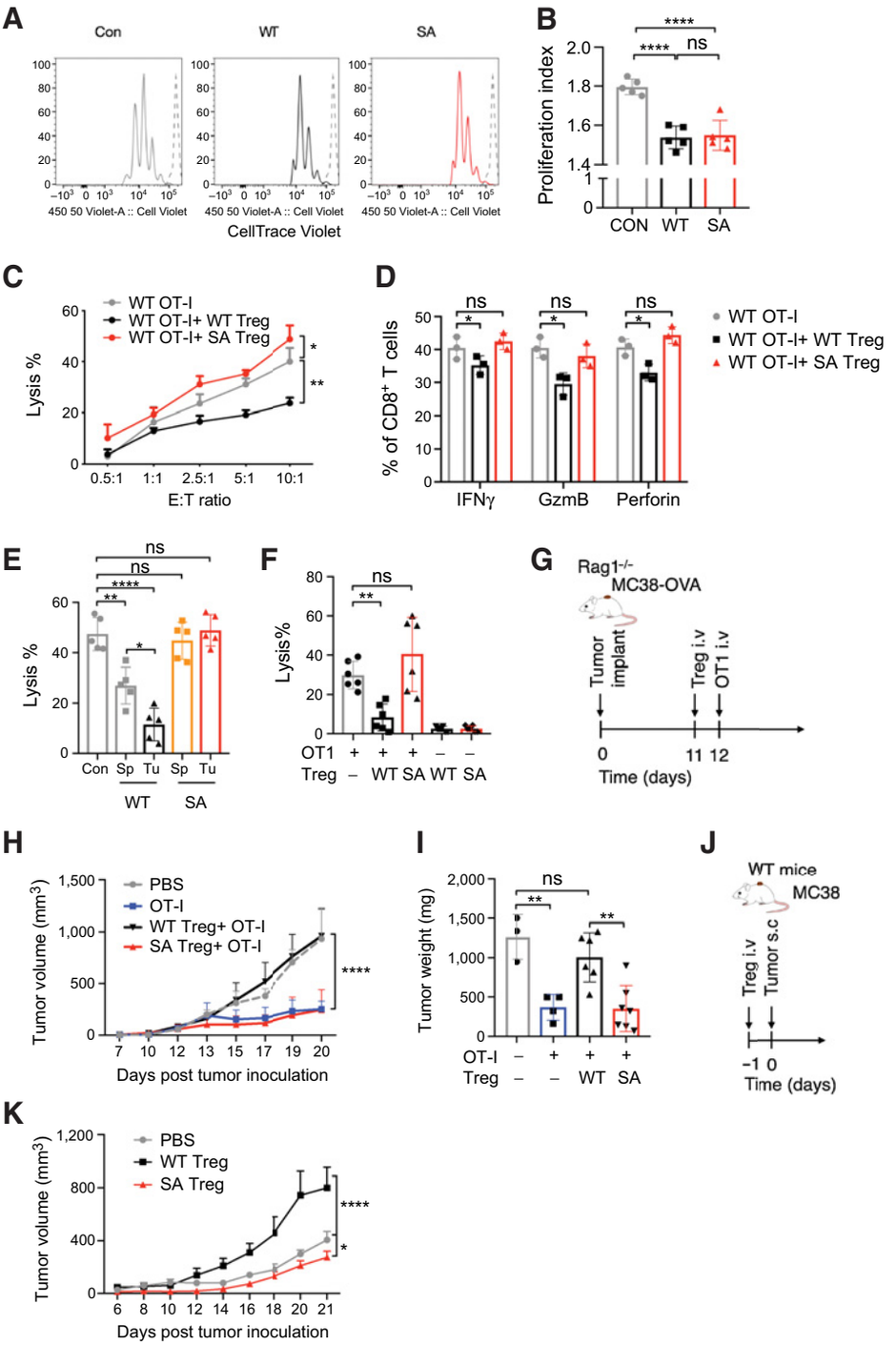

Figure 3.

Downregulation of IFNAR1 supports immune suppressive activities of Treg cells *in vitro* and *in vivo*. **A,** Representative flow cytometry analysis of *in vitro* proliferation of naïve WT CD8$^+$ T cells activated by magnetic beads precoated with agonist antibodies against CD3 and CD28 in the absence (Con) or presence of WT or SA iTregs (Treg:CD8 = 1:2 for 72 hours) as manifested by dilution of CellTrace Violet label. **B,** Quantification of the proliferation index of CD8$^+$ T cells described in **A** is presented as mean ± SEM ($n = 5$ samples). Statistical analysis was performed using ordinary one-way ANOVA with Tukey multiple comparisons test. ****, $P < 0.0001$. **C,** Percent lysis of MC38OVA-luc cells by OT-I CTL after coculture with or without WT or SA iTreg cells (Treg:OT-I = 1:3) at indicated tumor cell:CTL ratios. Data are shown as mean ± SEM ($n = 3$ samples). Statistical analysis was performed using two-way ANOVA with Tukey multiple comparisons test. *, $P = 0.0250$; **, $P = 0.0052$. **D,** Percent of OT-I cells positive for indicated cytokines/effector molecules after coincubation with WT or SA iTreg cells (Treg: OT-I = 1:3). Data are shown as mean ± SEM ($n = 3$ samples). Statistical analysis was performed using ordinary one-way ANOVA with Tukey multiple comparisons test. (*Continued on the following page.*)

We next sought to compare the immune suppressive activities of WT and SA cells. We generated iTregs by incubating naïve $CD4^+$ cells in the presence of TGFβ, which by itself was capable of reproducibly downregulating IFNAR1 in WT but not SA cells (Supplementary Fig. S2A). The expression of Foxp3 was comparable in WT and SA iTreg cells (Supplementary Fig. S2B and S2C). Furthermore, WT and SA iTregs exhibited similar levels of Helios, CTLA4, IL2, IL17, CD40 L, and Eos (Supplementary Fig. S2D). Compared with WT control, SA cells expressed greater levels of IFNAR1 and elevated Tbet and Helios (Supplementary Fig. S2C and S2D) but significantly lower levels of the negative regulator of fragility NRP1 and of the immune suppressive mediators TGFβ and CD73 (Supplementary Fig. S2E and S2F).

We further sought to determine the importance of IFNAR1 downregulation on the immune suppressive activities of iTreg cells *in vitro*. First, we used an assay that evaluated the ability of iTreg cells to elicit decreases in proliferation of $CD8^+$ T cells (as manifested by dilution of CellTrace Violet dye). Under these conditions, both WT and SA iTreg cells exhibited similar suppressive activity (**Fig. 3A** and **B**).

We next used an *in vitro* tumoricidal assay wherein the ability of iTreg cells to suppress killing of MC38OVA cells by OT-I CTL was analyzed. When conventional $CD4^+$ T cells (briefly treated or not with TGFβ to decrease IFNAR1 levels, as in Supplementary Fig. S2A) were added, they could not suppress the killing (Supplementary Fig. S3A). However, lysis of MC38OVA cells was notably attenuated by addition of WT iTreg cells (Supplementary Fig. S3A), unless they were pretreated with IFN1 (Supplementary Fig. S3B).

SA iTreg cells were incapable of protecting tumor cells from killing by CTL (**Fig. 3C**; Supplementary Fig. S3C) suggesting that inactivation of the IFN1–IFNAR1 pathway in iTreg cells supports their immune suppressive activities *in vitro*. Consistent with this result, the modest yet significant decrease in the percentage of OT-I CTL positive for IFNγ, granzyme B, or perforin that occurred upon coincubation with WT iTreg cells was not detected when we used SA iTreg cells (**Fig. 3D**).

To exclude the possibility that these results may artificially arise from the use of iTreg cells, we isolated Treg cells from spleens and MC38 tumors grown in WT or SA mice that harbor the *Foxp3-Cre-YFP* alleles and, accordingly, express yellow fluorescent protein (YFP) and Cre recombinase under the control of *Foxp3* promoter. Splenic WT YFP^+ but not SA YFP^+ Tregs significantly protected MC38OVA cells from killing by OT-I CTL (**Fig. 3E**). An even greater immune suppressive effect was elicited by intratumoral WT YFP^+ Treg cells. This phenotype was not observed for SA YFP^+ Treg cells (**Fig. 3E**) indicating that high levels of IFNAR1 is conducive to Treg-cell inactivation, whereas downregulation of IFNAR1 on WT intratumoral Treg cells may play a key role in maintaining their immune suppressive activities.

These conclusions were further supported by studies using intratumoral Treg cells isolated from MC38 tumors that were grown WT and SA mice, which expressed neither YFP nor Cre recombinase. Analysis of the suppressive activity of these cells revealed that intratumoral SA Treg cells were deficient in the ability to inhibit the killing activity of OT-I CTL (**Fig. 3F**) or to decrease their expression of IFNγ (Supplementary Fig. S3D). These data collectively suggest that downregulation of IFNAR1 on Treg cells supports their immunosuppressive properties in the tumor microenvironment.

Besides CTL, Treg cells can suppress a variety of immune cells (3, 19). Thus, we sought to determine the importance of IFNAR1 downregulation for immune suppressive activities of Treg cells *in vivo* using two independent models. First, we examined the ability of administered iTreg cells to attenuate the antitumor effects of adoptive transfer of tumor-specific CTL (**Fig. 3G**). In this setting, transfer of OT-I CTL robustly decelerated growth of MC38OVA tumors in *Rag1*-deficient mice. Coadministration of WT but not of SA iTregs prevented this therapeutic effect of OT-I CTL in this model (**Fig. 3H** and **I**).

In a second model, immunocompetent hosts received iTreg cells a day before subcutaneous inoculation of MC38 cells (**Fig. 3J**). Whereas WT iTreg cells significantly accelerated tumor growth, we did not observe this effect after administration of SA iTreg cells. In fact, a modest but significant deceleration of tumor growth was seen in this case (**Fig. 3K**; Supplementary Fig. S3E). Collectively, these *in vitro* and *in vivo* studies reveal that downregulation of IFNAR1 on Tregs is important for preserving the ability of these cells to suppress antitumor immune responses.

Downregulation of IFNAR1 in Treg cells protects them from fragility

We next focused on the mechanisms by which inactivation of IFNAR1 helps to maintain the immune suppressive activities of Treg cells. The scRNA-seq data had revealed an increased IFNγ signature in the intratumoral SA Treg cells (**Fig. 2C**). Therefore, we profiled gene expression in the iTreg cells. Similar to results from single-cell analysis of the tumor Treg cells, WT iTreg cells exhibited lower signatures not only for the IFN1 pathway but also for the IFNγ pathway (**Fig. 4A**). The latter results were validated by qPCR and flow cytometry analyses, which revealed a greater expression of *Ifng* mRNA (**Fig. 4B**) and protein (**Fig. 4C**) in SA iTreg cells compared with their WT counterparts.

High levels of IFNγ without loss of Foxp3 expression are characteristic of a few dysfunctional states of Treg cells including fragility (13). In NRP1-deficient mice, the Treg-cell fragility phenotype involves cytoplasmic retention and inactivation of FOXO3a (15). High levels of NRP1 have been found on human Treg cells from cancer patients and associated with poor prognosis (12).

(*Continued.*) *, $P < 0.05$. **E,** Percent lysis of MC38OVA-luc cells after incubation with OT-I CTL with or without Treg (Treg: OT-I = 1:3, E:T = 10:1) cells (YFP^+) isolated from spleen (Sp) or tumors (Tu) from *Foxp3-Cre* WT or *Foxp3-Cre* SA MC38 tumor–bearing mice (day 16 after tumor injection). Data are shown as mean ± SEM ($n = 6$ samples). Statistical analysis was performed using ordinary one-way ANOVA with Tukey multiple comparisons test. *, $P = 0.0143$; **, $P = 0.0011$; ****, $P < 0.0001$. **F,** Percent lysis of MC38OVA-luc cells after incubation with OT-I CTL with or without Treg cells isolated from MC38 tumors growing in WT or SA mice (day 20 after tumor injection, Treg: OT-I = 1:3, E:T = 10:1). Data are shown as mean ± SEM ($n = 6$ samples). Statistical analysis was performed using ordinary one-way ANOVA with Tukey multiple comparisons test. **, $P = 0.0049$. **G,** Schematic depiction of experiment to test comparative immunosuppressive activities of WT and SA Treg cells (iTreg, 2.5×10^6/mouse) administered into MC38OVA tumor-bearing immunocompromised host *in vivo* before adoptive transfer of OT-I CTL (5×10^6/mouse). **H,** Volume of MC38OVA subcutaneous tumors in mice described in **G**. Data are shown as mean ± SEM ($n = 3$–6 mice). Statistical analysis was performed using two-way ANOVA with Tukey multiple comparisons test. ****, $P < 0.0001$. **I,** Tumor weight of MC38OVA tumors grown in mice described in **G**. Data are shown as mean ± SEM ($n = 3$–6 mice). Statistical analysis was performed using ordinary one-way ANOVA with Tukey multiple comparisons test. **, $P < 0.01$. **J,** Schematic depiction of experiment to test comparative immunosuppressive activities of WT and SA iTreg cells (10^6/mouse) administered into C57BL/6 hosts before inoculation of MC38 tumors (s.c., 10^6/mouse). **K,** Volume of MC38 subcutaneous tumors in mice described in **J**. Data are shown as mean ± SEM ($n = 3$–4 mice). Statistical analysis was performed using two-way ANOVA with Tukey multiple comparisons test. *, $P = 0.0295$; ****, $P < 0.0001$.

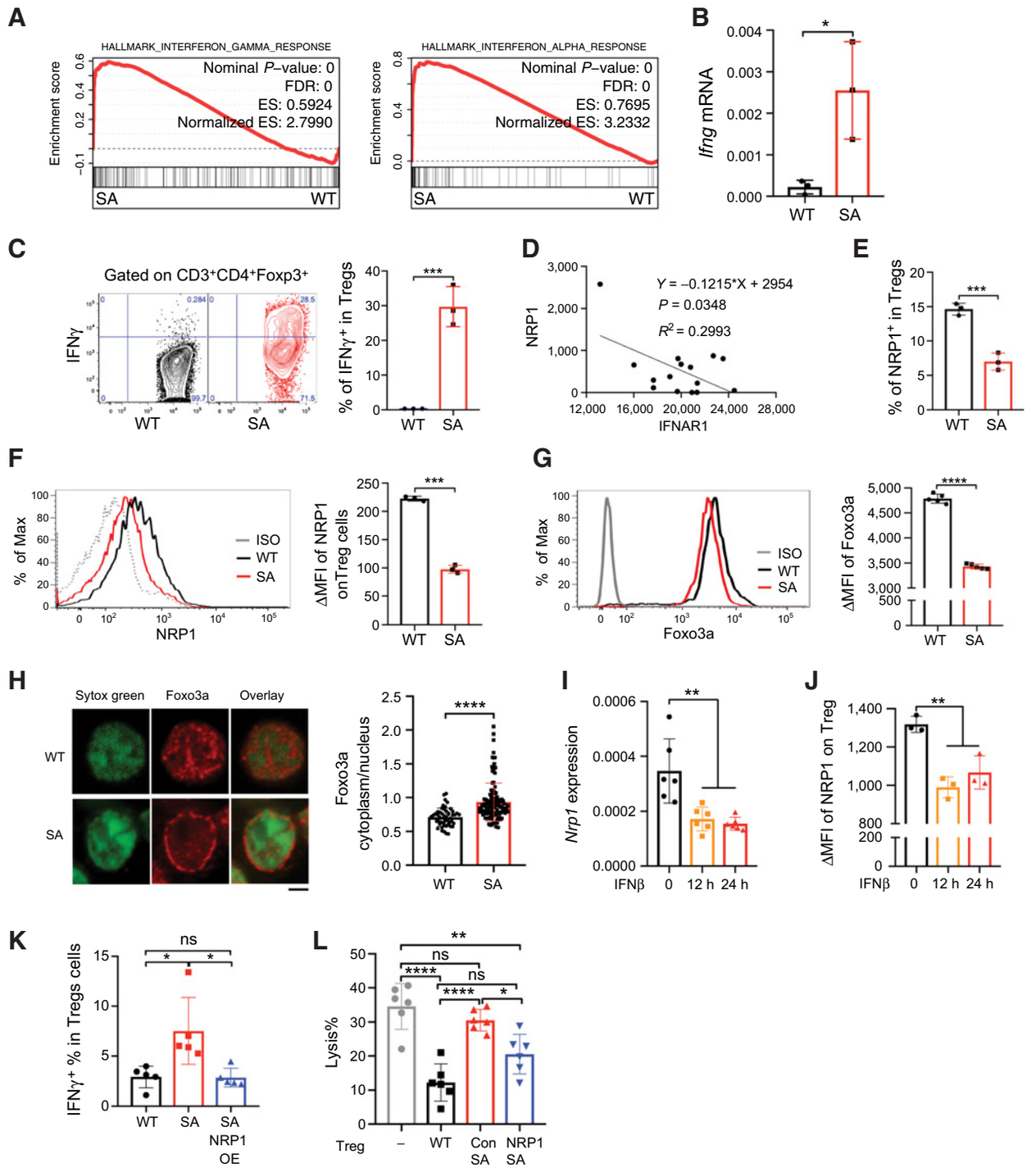

Figure 4.

Stabilization of IFNAR1 induces iTreg fragility *in vitro.* All the iTreg cells used in this figure were used right after differentiation *in vitro* and without restimulation before experiments. **A,** WT and SA iTreg cells were induced *in vitro* accordingly. RNA sequencing analysis of Leading-edge plots depicting the results of GSEA of indicated gene expression signatures in WT and SA iTreg. **B,** qPCR analysis of mRNA for *Ifng* in the indicated mouse iTreg cells. Data are shown as mean ± SEM ($n = 3$ mice). Two-tailed unpaired *t* test was performed for the comparisons between groups. *, $P = 0.0351$. **C,** Flow cytometry analysis of IFNγ levels in indicated iTreg cells. Quantification of the percent IFNγ$^+$ cells among the iTregs (on the right) is shown as mean ± SEM ($n = 3$ mice). Two-tailed unpaired *t* test was performed for the comparisons between groups. ***, $P = 0.0009$. **D,** Flow cytometry analysis of IFNAR1 and NRP1 protein levels in Treg cells (CD4$^+$Foxp3$^+$) from human tumor patients' blood samples. $n = 15$ samples. Linear reg. of Correlation was performed. **E,** Flow cytometry analysis showing percent of NRP1$^+$ cells among the indicated iTreg cells. Data are shown as mean ± SEM ($n = 3$ mice). Two-tailed unpaired *t* test was performed for the comparisons between groups. (*Continued on the following page.*)

We examined the levels of IFNAR1 and NRP1 on the surface of Treg cells ($CD4^+FOXP3^+$) from blood of patients with cancer. This analysis revealed that expression of NRP1 displayed an inverse correlation with IFNAR1 (**Fig. 4D**). Likewise, a greater number of $NRP1^+$ cells and increased cell surface NRP1 levels were found in mouse WT iTreg cells compared with SA iTreg cells (**Fig. 4E** and **F**, Supplementary Fig. S4A). Compared with WT control iTreg cells, SA iTreg cells expressed lower levels (**Fig. 4G**) and cytoplasmic retention (**Fig. 4H**) of FOXO3a protein. These results indicate that downregulation of IFNAR1 and ensuing inactivation of the IFN1 pathway may play an important role in the maintenance of the NRP1–FOXO3a pathway and protection of Treg cells from fragility.

Treatment of $CD4^+$ EL4 murine thymoma cells with IFNβ decreased levels of NRP1 (Supplementary Fig. S4B). Furthermore, IFNβ treatment of WT Treg cells significantly downregulated their levels of *Nrp1* mRNA (**Fig. 4I**) and protein (**Fig. 4J**). To determine the importance of modulation of NRP1 levels by the IFN1–IFNAR1 pathway, we sought to rescue the SA fragility phenotype by transducing SA iTreg cells with NRP1-expressing construct (Supplementary Fig. S4C). This transduction did not affect levels of either IFNAR1 or FOXP3 (Supplementary Fig. S4D). However, reexpression of NRP1 in SA iTreg cells significantly decreased the percentage of $IFN\gamma^+$ cells (**Fig. 4K**) and partially restored their ability to interfere with the killing activity of OT-I CTL (**Fig. 4L**). These results suggest that inactivation of the IFN1–IFNAR1 pathway contributes to the maintenance of NRP1 expression in Treg cells and enables immune suppressive activities of these cells.

We next analyzed NRP1 and IFNγ expression in Tregs *in vivo* (Supplementary Fig. S5A). In line with the proposed role of IFNAR1 downregulation in protection of the intratumoral Tregs from fragility, we observed higher levels of NRP1 and lower IFNγ expression in intratumoral Treg cells compared with splenic Treg cells from tumor-bearing WT mice. This phenotype was not observed in MC38 tumor–bearing SA mice (**Fig. 5A** and **B**) thereby supporting current hypothesis.

In a separate set of experiments, we analyzed fragility of intratumoral WT and SA Treg cells from MC38, CT26, and B16F10 tumors. In all described tumor models, these studies demonstrated that intratumoral SA Treg cells exhibited significantly increased levels of IFNγ (**Fig. 5C–E**) and significantly decreased $NRP1^+$ frequencies (**Fig. 5F–H**) and levels of NRP1 (**Fig. 5I–K**) compared with WT Treg cells. These results suggest that downregulation of IFNAR1 in the intratumoral Treg cells maintains expression of NRP1 and protects them from fragility in the tumor microenvironment.

Reactivating IFNAR1 in Treg cells induces their fragility and suppresses tumor growth

We next aimed to control fragility of Treg cells by modulating their IFNAR1 levels. The phosphorylation of IFNAR1 that drives its ubiquitination and degradation is mediated by p38α protein kinase (encoded by the *Mapk14* gene), which is activated by tumor-derived factors and stress stimuli in the tumor microenvironment (23, 31). We generated $Mapk14^{\Delta Foxp3}$ mice, which lack p38α kinase in Treg cells. Splenic Treg cells from these mice exhibited higher levels of IFNAR1 but similar levels of FOXP3 and of many other markers including NRP1, IL2, CTLA4, Tbet, Helios, Eos, and Ki-67 (Supplementary Fig. S6A).

Analysis of MC38 tumors grown in $Mapk14^{\Delta Foxp3}$ mice revealed no significant differences in the intratumoral frequencies or numbers of Treg cells or CTL compared with WT mice (Supplementary Fig. S6B–S6F). However, the intratumoral CTL in these mice manifested a significantly greater expression of IFNγ (**Fig. 6A**) suggesting increased activity, which could be a result of inactivation of p38α-deficient Treg cells.

Frequencies of $IFN\gamma^+$ intratumoral Treg cells were increased in $Mapk14^{\Delta Foxp3}$ mice bearing MC38 tumors compared with intratumoral Treg cells from WT mice (**Fig. 6B**). Treg cell–specific ablation of *Mapk14* also led to upregulation of IFNAR1 (**Fig. 6C**) and downregulation of NRP1 (**Fig. 6D**) indicating that p38α kinase is a negative regulator of fragility in Treg cells. Furthermore, a significant deceleration of tumor growth (**Fig. 6E**; Supplementary Fig. S6G) and improved survival (**Fig. 6F**) in tumor-bearing $Mapk14^{\Delta Foxp3}$ mice compared with WT mice indicate the importance of p38α-dependent suppression of Treg fragility in the protumorigenic function of these cells.

All the phenotypes associated with p38α ablation in Tregs were significantly attenuated or even outright reversed by additional genetic ablation of the *Ifnar1* alleles in Foxp3-expressing cells ($Ifnar1^{\Delta Foxp3}Mapk14^{\Delta Foxp3}$; **Fig. 6A–F**; Supplementary Fig. S6G). These results collectively indicate that p38α-dependent downregulation of IFNAR1 on Treg cells protects them from fragility and promotes immune suppression and tumor growth. Additional support for these conclusions came from experiments using selective p38α inhibitor ralimetinib (LY2228820). Administration of this agent *in vivo* notably inhibited growth of MC38 tumors and increased survival of tumor-bearing WT animals, but these effects were not observed in mice lacking IFNAR1 in Treg cells ($Ifnar1^{\Delta Foxp3}$; **Fig. 6G** and **H**; Supplementary Fig. S6H), indicating that regulation of Treg-cell IFNAR1 is instrumental in the antitumor activities of ralimetinib.

As a complementary approach, we used a novel, potent, and specific inhibitor of protein sumoylation, TAK981, which is currently being tested in anticancer clinical trials (including NCT03648372, NCT04074330, NCT04381650, and NCT04776018). The rationale for this approach included the fact that sumoylation is important for Treg-cell expansion and function (32) and the knowledge that TAK981 can induce expression of IFN1, upregulate IFNAR1 levels and reactivate the IFN1–IFNAR1 pathway in the immune cells of the tumor microenvironment (28). Treatment of iTreg cells with TAK981 upregulated IFNAR1 (**Fig. 7A**) and IFNγ (**Fig. 7B**), and decreased expression of NRP1 (**Fig. 7C**). Furthermore, pretreatment of WT iTreg cells with TAK981 prevented the ability of these cells to suppress killing activity of OT-I CTL (**Fig. 7D**). Moreover, *Ifnar1*-deficient iTreg cells

(*Continued.*) ***, $P = 0.0008$. **F,** Flow cytometry analysis of NRP1 levels in indicated iTregs. Quantification data (on the right) are shown as mean ± SEM ($n = 3$ mice). Two-tailed unpaired *t* test was performed for the comparisons between groups. ***, $P = 0.0001$. **G,** Flow cytometry analysis of FOXO3a levels in indicated iTregs. Quantification data (on the right) are shown as mean ± SEM ($n = 5$ mice). Two-tailed unpaired *t* test was performed for the comparisons between groups. ****, $P < 0.0001$. **H,** Confocal analysis of FOXO3a in the cytoplasm and nuclei (highlighted by Sytox Green staining of DNA) in WT and SA iTreg cells. Scale bar, 2 μm. Quantification data (on the right) are shown as mean ± SEM ($n = 5$ for mice). Two-tailed unpaired *t* test was performed for the comparisons between groups. ****, $P < 0.0001$. **I,** qPCR analysis of mRNA for *Nrp1* in WT iTreg cells treated with mIFNβ (1,000 IU/mL) for indicated time points. Data are shown as mean ± SEM ($n = 6$ samples). Statistical analysis was performed using ordinary one-way ANOVA with Tukey multiple comparisons test. **, $P < 0.01$. **J,** Flow cytometry analysis of NRP1 levels in WT iTreg cells treated with mIFNβ (1,000 IU/mL) for indicated timepoints. Data are shown as mean ± SEM ($n = 3$ mice). Statistical analysis was performed using ordinary one-way ANOVA with Tukey multiple comparisons test. **, $P < 0.01$. **K,** Flow cytometry analysis of $IFN\gamma^+$ iTreg cells (WT, SA, and SA overexpressing NRP1). Data are shown as mean of percent $IFN\gamma^+$ cells among the iTreg cells ± SEM ($n = 5$ samples). Statistical analysis was performed using ordinary one-way ANOVA with Tukey multiple comparisons test. *, $P < 0.05$.

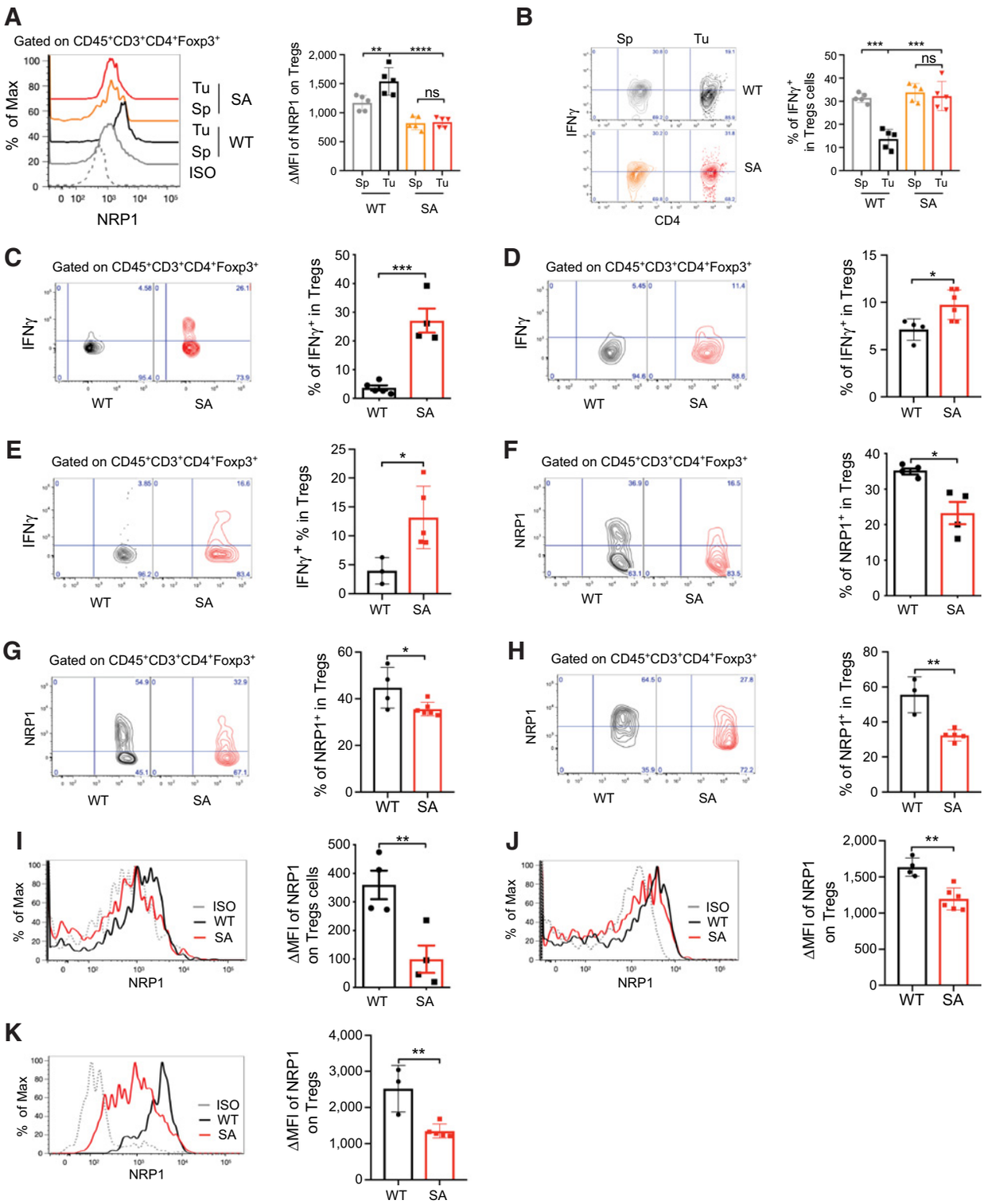

Figure 5.

Stabilization of IFNAR1 induces Treg fragility *in vivo*. **A,** Flow cytometry analysis of NRP1 levels on Treg cells ($CD45^+CD3^+CD4^+Foxp3^+$) from tumor and spleen from WT mice on day 14 after inoculation of subcutaneous MC38 cells (1×10^6 cells/mouse). Data are shown as mean ± SEM ($n = 5$ mice). Statistical analysis was performed using ordinary one-way ANOVA with Tukey multiple comparisons test. **, $P = 0.0069$; ****, $P < 0.0001$. **B,** Flow cytometry analysis of $IFN\gamma^+$ Treg cells from tumor and spleen samples analyzed in **A**. Data are shown as mean ± SEM ($n = 5$ mice). (*Continued on the following page.*)

exhibited a greater suppressive activity and were insensitive to the effects of TAK981 in this assay (**Fig. 7D**). These results suggest that TAK981 can induce fragility in Treg cells and subvert their immune suppressive activities in an IFNAR1-dependent manner.

Consistent with these *in vitro* data, administration of TAK981 to MC38 tumor-bearing mice (**Fig. 7E**) significantly suppressed tumor growth (**Fig. 7F**) and prolonged animal survival (**Fig. 7G**). The therapeutic efficacy of TAK981 was eliminated in *Ifnar1*$^{\Delta Foxp3}$ mice, which lack IFNAR1 on their Treg cells (**Fig. 7F** and **G**) suggesting that reactivation of the IFN1–IFNAR1 pathway in Treg cells contributes to the mechanism of action of TAK981. Furthermore, analysis of Treg cells isolated from mice inoculated with MC38 cells in a separate experiment (Supplementary Fig. S7A–S7C) revealed that TAK981 induced fragility of the intratumoral Treg cells as manifested by an increase in IFNAR1 and IFNγ and decrease in NRP1 levels (**Fig. 7H–J**; Supplementary Fig. S7D–S7F). In all, these results suggest that TAK981-induced inactivation of Treg cells impedes their immune suppressive protumorigenic activities.

Discussion

Intratumoral Treg cells are protected from inactivation via downregulation of IFNAR1

The suppressive functions of Treg cells are tempered in inflamed tissues (14, 33). However, Treg cells exhibit immune suppressive and protumorigenic activities inside solid tumors, which are brimming with proinflammatory stimuli including IFN1 (2, 34). Thus, it is important to understand how Treg cells can function in the tumor microenvironment. The mechanisms by which intratumoral Treg cells are protected from inactivation are expected to play an important role in tumor growth and progression and, conversely, represent a potential target for anticancer therapies.

Tumor microenvironment–associated stimuli act to downregulate IFNAR1 on many types of intratumoral cells including malignant cells (30), CTL (25), myeloid-derived suppressor cells (35), and cancer-associated fibroblasts (36). Many factors present in the tumor microenvironment are redundant in triggering downregulation of IFNAR1 and inhibition of the IFN1–IFNAR1 pathways. These factors include inflammatory cytokines [e.g., IL1α/β (23)], integrated stress response (24), tumor-derived extracellular vesicles (22), VEGF (37), and TGFβ (this study). These stimuli are known to activate p38α kinase (38).

Here we demonstrate that p38α-mediated IFNAR1 downregulation occurs on intratumoral Treg cells, enabling these cells to maintain the expression of NRP1, protecting them from fragility and stimulating their immune suppressive and protumorigenic activities. These genetic and pharmacologic studies identify and characterize p38α kinase as a critical regulator of Treg function in cancer. Future studies are required to examine the potential links of p38α with other recently identified factors that control fragility of intratumoral Treg cells including the alarmin IL33 (39) and the CARMA1–BCL10–MALT1 signalosome complex (40).

Under several biological and pathologic scenarios, inactivation of Treg cells can occur through the loss of FOXP3 stability or via fragility (13, 14). The p38α-driven downregulation of IFNAR1 apparently affects the latter mechanism given that *Map14*-deficient and SA Treg cells preserve expression of FOXP3 and other markers of Treg cells. In addition, the regulatory phenotype can be partially restored in SA Tregs by reexpression of NRP1. Furthermore, SA mice do not exhibit deleterious autoimmune phenotypes seen in FOXP3-deficient scurfy mice (6, 7). It is tempting to speculate that temporary downregulation of IFNAR1 in inflamed tissues (e.g., tumors) enables Treg cells to acquire a defined epigenetic "memory" (33) that supports their immune suppressive function. Conversely, upon exit from the inflammatory environment, Treg cells are expected to reexpress IFNAR1 and eventually reduce their regulatory potential.

Mechanisms underlying the roles of the IFN1–IFNAR1 pathway in Treg fragility

On the basis of our data demonstrating that SA Treg cells engineered to reexpress NRP1 do not downregulate IFNAR1 yet exhibit partially restoration of their immune suppressive activities, we propose that IFN1-induced decreases in NRP1 expression play an important role in inactivation of Tregs. However, given that tonic IFN1–IFNAR1 signaling can upregulate STAT1, which in turn would augment responses to IFNγ (41), we cannot rule out the NRP1-independent contribution of IFN1 to the fragility phenotype. Future studies will determine how IFN1 acts to decrease levels of TGFβ and NRP1 in Treg cells. Furthermore, in the context of our studies, a decrease in levels of TGFβ and CD73 may contribute to the mechanisms by which the IFN1–IFNAR1 pathway attenuates the immune suppressive activities of Treg cells. However, given important role of IL10 and IL35 in NRP1-dependent suppressive activities (15), additional mechanisms should not be ruled out and warrant further studies.

Current literature on the roles of IFNAR1 in the biology of Treg cells is complex and somewhat contentious. Whereas knockout of IFNAR1 undermined Treg-cell function within the context of a Scurfy disease model (42), an increase in Treg-cell activation and proliferation has

(*Continued.*) Statistical analysis was performed using ordinary one-way ANOVA with Tukey multiple comparisons test. ***, $P < 0.001$. **C,** Flow cytometry analysis of IFNγ$^+$ Treg cells in tumor tissues from WT or SA mice on day 14 after inoculation of subcutaneous MC38 tumors (1×10^6 cells/mouse). Data are shown as mean of percent IFNγ$^+$ cells among the Treg cells ± SEM ($n = 4$–6 mice). Two-tailed unpaired *t* test was performed for the comparisons between groups. ***, $P = 0.0005$. **D,** Flow cytometry analysis of IFNγ$^+$ Treg cells in tumor tissues from WT or SA mice on day 13 after inoculation of subcutaneous CT26 tumors (1×10^6 cells/mouse). Data are shown as mean of percent IFNγ$^+$ cells among the Treg cells ± SEM ($n = 4$–6 mice). Two-tailed unpaired *t* test was performed for the comparisons between groups. *, $P = 0.0212$. **E,** Flow cytometry analysis of IFNγ$^+$ Treg cells in tumor tissues from WT or SA mice on day 15 after inoculation of subcutaneous B16F10 tumors (1×10^6 cells/mouse). Data are shown as mean of percent IFNγ$^+$ cells among the Treg cells ± SEM ($n = 3$–5 mice). Two-tailed unpaired *t* test was performed for the comparisons between groups. *, $P = 0.0333$. **F,** Flow cytometry analysis of NRP1$^+$ Treg cells from tumor samples analyzed in **C**. Data are shown as mean of percent NRP1$^+$ cells among the Treg cells ± SEM ($n = 3$–5 mice). Two-tailed unpaired *t* test was performed for the comparisons between groups. *, $P = 0.0103$. **G,** Flow cytometry analysis of NRP1$^+$ Treg cells from tumor samples analyzed in **D**. Data are shown as mean of percent NRP1$^+$ cells among the Treg cells ± SEM ($n = 4$–6 mice). Two-tailed unpaired *t* test was performed for the comparisons between groups. *, $P = 0.0400$. **H,** Flow cytometry analysis of NRP1$^+$ Treg cells from tumor samples analyzed in **E**. Data are shown as mean of percent NRP$^+$ cells among the Treg cells ± SEM ($n = 3$–5 mice). Two-tailed unpaired *t* test was performed for the comparisons between groups. **, $P = 0.0028$. **I,** Flow cytometry analysis of NRP1 levels in Treg cells from tumor samples analyzed in **C**. Data are shown as mean ± SEM ($n = 4$–6 mice). Two-tailed unpaired *t* test was performed for the comparisons between groups. **, $P = 0.0095$. **J,** Flow cytometry analysis of NRP1 levels in Treg cells from tumor samples analyzed in **D**. Data are shown as mean ± SEM ($n = 4$–6 mice). Two-tailed unpaired *t* test was performed for the comparisons between groups. **, $P = 0.0014$. **K,** Flow cytometry analysis of NRP1 levels in Treg cells from tumor samples analyzed in **E**. Data are shown as mean ± SEM ($n = 3$–5 mice). Two-tailed unpaired *t* test was performed for the comparisons between groups. **, $P = 0.0072$.

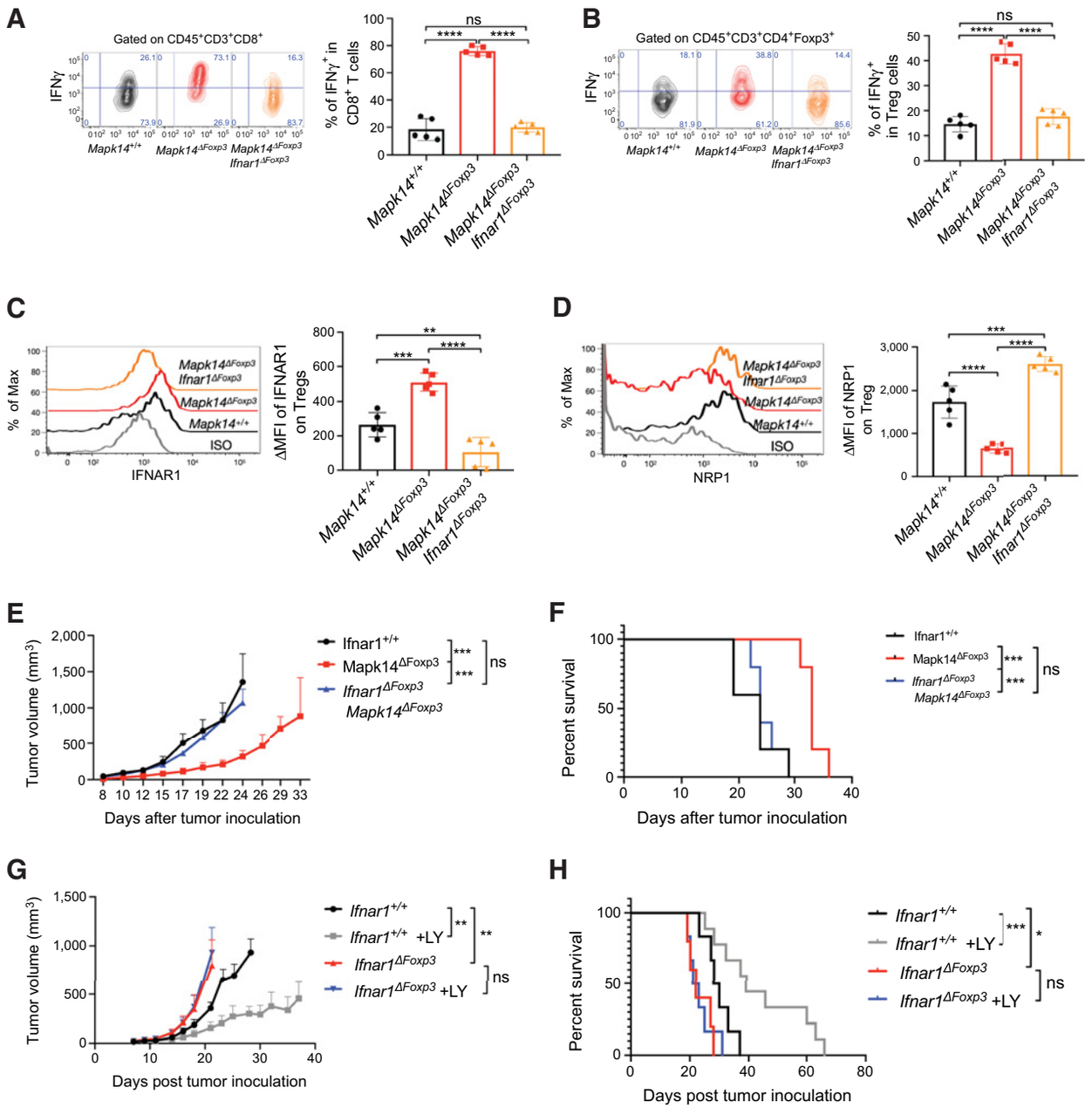

Figure 6.

Treg fragility is regulated by p38α kinase in an IFNAR1-dependent manner. **A,** Flow cytometry analysis of IFNγ$^+$ CTLs (CD45$^+$CD3$^+$CD8$^+$) in tumor tissues from *Mapk14*$^{+/+}$, *Mapk14*$^{\Delta Foxp3}$, and *Mapk14*$^{\Delta Foxp3}$*Ifnar1*$^{\Delta Foxp3}$ mice on day 14 after inoculation of subcutaneous MC38 tumors (1×10^6 cells/mouse). Data are shown as mean of percent IFNγ$^+$ cells among the CTLs ± SEM ($n = 5$ mice). Statistical analysis was performed using ordinary one-way ANOVA with Tukey multiple comparisons test. ****, $P < 0.0001$. **B,** Flow cytometry analysis of IFNγ$^+$ Tregs in tumor tissues described in **A**. Data are shown as mean of percent IFNγ$^+$ cells among the Treg cells ± SEM ($n = 5$ mice). Statistical analysis was performed using ordinary one-way ANOVA with Tukey multiple comparisons test. ****, $P < 0.0001$. **C,** Flow cytometry analysis of IFNAR1 levels in Tregs in tumor tissues described in **A**. Data are shown as mean ± SEM ($n = 5$ mice). Statistical analysis was performed using ordinary one-way ANOVA with Tukey multiple comparisons test. **, $P = 0.0096$; ***, $P = 0.0003$; ****, $P < 0.0001$. **D,** Flow cytometry analysis of NRP1 levels in Tregs in tumor tissues described in **A**. Data are shown as mean ± SEM ($n = 5$ mice). Statistical analysis was performed using ordinary one-way ANOVA with Tukey multiple comparisons test. ***, $P = 0.0003$; ****, $P < 0.0001$. **E,** Volume of MC38 subcutaneous tumors (5×10^5 cells/mouse) in mice of indicated genotypes. Data are shown as mean ± SEM ($n = 5$ mice/genotype). Statistical analysis was performed using two-way ANOVA with Tukey multiple comparisons test. ***, $P < 0.001$. **F,** The Kaplan–Meier analysis of survival of animals from the experiment described in **D** ($n = 5$ mice). Statistical analysis was performed using log-rank (Mantel–Cox) test. ***, $P < 0.001$. **G,** Volume of MC38 tumors (5×10^5 cells/mouse, s.c.) in *Ifnar1*$^{+/+}$ and *Ifnar1*$^{\Delta Foxp3}$ mice that were administered LY (LY, 10 mg/kg) or vehicle by oral gavage every other day from day 7 after inoculation. Data are shown as mean ± SEM ($n = 5$–9 mice). Statistical analysis was performed using two-way ANOVA with Tukey multiple comparisons test. **, $P < 0.01$. **H,** The Kaplan–Meier analysis of survival of animals from experiment described in **G** ($n = 5$–9 mice). Statistical analysis was performed using log-rank (Mantel–Cox) test. *, $P = 0.0225$; ***, $P = 0.0002$.

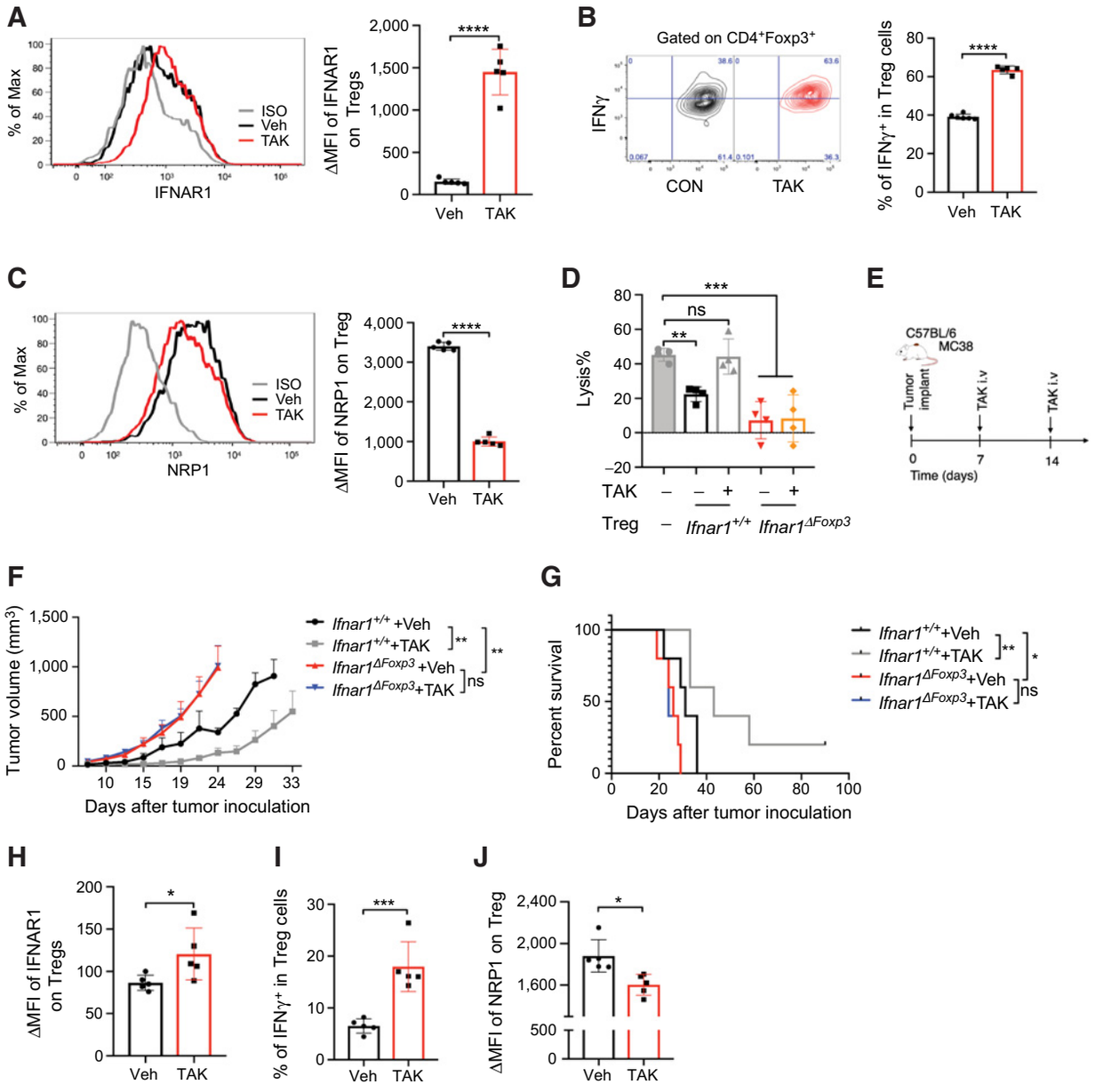

Figure 7.

Sumoylation inhibitor TAK981 induces Treg fragility and suppresses tumor growth in a manner dependent on expression of IFNAR1 in Treg cells. **A,** Flow cytometry analysis of IFNAR1 levels on WT iTreg cells treated with or without TAK981 (100 nmol/L in DMSO, 24 hours). Data are shown as mean ± SEM ($n = 5$ samples). Two-tailed unpaired *t* test was performed for the comparisons between groups. ****, $P < 0.0001$. **B,** Flow cytometry analysis of IFNγ$^+$ Tregs treated as in A. Data are shown as mean ± SEM ($n = 5$ samples). Two-tailed unpaired *t* test was performed for the comparisons between groups. ****, $P < 0.0001$. **C,** Flow cytometry analysis of NRP1 levels on Tregs treated as in A. Data are shown as mean ± SEM ($n = 5$ samples). Two-tailed unpaired *t* test was performed for the comparisons between groups. ****, $P < 0.0001$. **D,** Percent lysis of MC38OVA-Luc cells after incubation with OT-I CTL with or without indicated (*Ifnar1*$^{+/+}$ or *Ifnar1*$^{\Delta Foxp3}$) iTreg cells (Treg: OT-I = 1:3, E:T = 10:1)treated with or without TAK981 (100 nmol/L, 24 hours). ($n = 4$ samples). Statistical analysis was performed using ordinary one-way ANOVA with Tukey multiple comparisons test. *, $P = 0.0256$; ***, $P < 0.001$. **E,** Schematic depiction of experiment to analyze the effects of TAK981 on tumor growth and status of Treg cells. MC38 (5×10^5/mouse) were inoculated subcutaneously into syngeneic mice treated as indicated. **F,** Volume of MC38 tumor growth in *Ifnar1*$^{+/+}$ or *Ifnar1*$^{\Delta Foxp3}$ mice treated with or without TAK981 at d7 and d14 (15 mg/kg, i.v.) as shown in E. ($n = 5$ mice/group). Statistical analysis was performed using two-way ANOVA with Tukey multiple comparisons test. **, $P < 0.01$. **G,** The Kaplan–Meier analysis of survival of animals from experiments described in **E** and **F**. ($n = 5$ mice). Statistical analysis was performed using log-rank (Mantel–Cox) test. *, $P = 0.0471$; **, $P = 0.0034$. **H,** Flow cytometry analysis of IFNAR1 levels on Tregs isolated from MC38 tumors growing in C57BL/6 WT mice treated with or without TAK981 (15 mg/kg, i.v. at day 7 and day 14). Data are shown as mean ± SEM ($n = 5$ mice). Two-tailed unpaired *t* test was performed for the comparisons between groups. *, $P = 0.0451$. **I,** Flow cytometry analysis of IFNγ$^+$ Tregs isolated from MC38 tumors described in **H**. Data are shown as mean ± SEM ($n = 5$ mice). Two-tailed unpaired *t* test was performed for the comparisons between groups. ***, $P = 0.0009$. **J,** Flow cytometry analysis of NRP1 levels on Tregs isolated from MC38 tumors described in **H**. Data are shown as mean ± SEM ($n = 5$ mice). Two-tailed unpaired *t* test was performed for the comparisons between groups. *, $P = 0.0104$.

been reported in IFNAR1-deficient mice under conditions of viral infection or tumor growth (43, 44). Studies in *Ifnar1*$^{\Delta Foxp3}$ mice growing B16F10 solid melanoma tumors demonstrate that inactivation of IFNAR1 in Treg cells augments their immune suppressive properties and increases their ability to stimulate tumor growth (44). Our control experiments using studies in SA mice as well as the same *Ifnar1*$^{\Delta Foxp3}$ mouse model challenged with B16F10 (along with MC38 and CT26) tumors support these conclusions.

However, different results were obtained in a model of hematologic malignancy (45). It was reported that myeloma cells produce IFNβ, which in turn activates the IFN1–IFNAR1 pathway in bone marrow Treg cells. Furthermore, antibody-mediated neutralization of IFNAR1 decreased Treg-cell function and inhibited myeloma progression (45). Besides variations in approaches to modulating IFNAR1, this discourse may stem from specific biological properties of myeloma cells as well as different characteristics of the tumor microenvironment in a solid tumor versus bone marrow. Given these complexities, additional clarification of the roles of IFN1 and IFNAR1 in the biology of Treg cells in hematologic malignancies is needed to better understand the therapeutic potential of these and our studies.

Prospective anticancer therapeutic strategies to induce fragility of Treg cells

Identification and targeting factors that support the immune suppressive function of Treg cells in cancers is expected to yield novel means for anticancer therapies (3, 4, 13, 19). Several therapeutic strategies have been proposed to counteract Treg cell–mediated immunosuppression. However, these approaches, including depletion of Treg cells using antibodies against CD25 (daclizumab) or CCR4 (mogamulizumab), encountered limitations in clinical settings (19).

An alternative therapeutic approach may rely upon induction of fragility and inactivation of Treg cells. Our data demonstrating induction of Treg fragility by pharmacologic agents stabilizing IFNAR1, such as the p38α inhibitor ralimetinib and a novel sumoylation inhibitor TAK981, provide a proof of principle for targeting this mechanism for anticancer therapies. TAK981 was previously shown to reactivate the IFN1–IFNAR1 pathway in the intratumoral immune cells (28). Moreover, TAK981 can upregulate IFNAR1 on Treg cells, and the therapeutic effects of TAK981 require IFNAR1 expression on these cells. Treg-cell fragility plays an important role in shaping positive responses of patients with cancer to immune checkpoint inhibitors (12, 13) and TAK981 has been shown to robustly augment the efficacy of inhibitors of PD-1 and CTLA4 (28). Our current results also argue for additional preclinical and clinical studies combining TAK981 or other agents inducing Treg fragility with immune therapies.

Authors' Disclosures

Y. Nefedova reports grants from NIH/NCI during the conduct of the study; grants and non-financial support from Active Biotech, Jubilant Therapeutics, Merck, and Buzzard Pharmaceuticals; non-financial support from BMS outside the submitted work. J.R. Conejo-Garcia reports personal fees from Alloy Therapeutics and grants and personal fees from Anixa Biosciences outside the submitted work; and Compass Therapeutics: Intellectual property, stock options; Alloy Therapeutics: Stock options; Anixa Biosicences: Intellectual property, stock options, all outside the scope of this work. D.I. Gabrilovich reports other support from AstraZeneca outside the submitted work. S.Y. Fuchs reports grants from NIH during the conduct of the study. No disclosures were reported by the other authors.

Authors' Contributions

H. Zhang: Conceptualization, formal analysis, investigation, methodology, writing–original draft, writing–review and editing. **V.S. Tomar:** Data curation, formal analysis, investigation. **J. Li:** Data curation, software, formal analysis, validation, investigation, methodology, writing–original draft. **R. Basavaraja:** Investigation, methodology. **F. Yan:** Data curation, software, formal analysis, investigation. **J. Gui:** Data curation, formal analysis, investigation, writing–original draft. **N. McBrearty:** Data curation, investigation. **T.L. Costich:** Resources, formal analysis, investigation. **D.P. Beiting:** Data curation, software, formal analysis, validation, investigation, methodology. **M.A. Blanco:** Data curation, software, formal analysis, supervision. **J.R. Conejo-Garcia:** Resources, formal analysis, supervision, investigation, writing–review and editing. **G. Saggu:** Resources, data curation, writing–review and editing. **A. Berger:** Resources, data curation, writing–review and editing. **Y. Nefedova:** Resources, supervision, funding acquisition, writing–review and editing. **D.I. Gabrilovich:** Conceptualization, formal analysis, investigation, writing–original draft, writing–review and editing. **S.Y. Fuchs:** Conceptualization, resources, supervision, writing–original draft, project administration, writing–review and editing.

Acknowledgments

This work was supported by the by the NIH/NCI R01 grant no. CA216936 (to Y. Nefedova and S.Y. Fuchs), grant no. CA247803 (to S.Y. Fuchs) as well as by additional support from T32 grant no. CA115299 (to N. McBrearty). We thank Dr. Suzanne Ostrand-Rosenberg (University of Maryland) and Yibin Wang (UCLA) for the reagents, and A. Gamero (Temple University) and the members of the Gabrilovich, Fuchs, and Nefedova laboratories for critical suggestions.

The publication costs of this article were defrayed in part by the payment of publication fees. Therefore, and solely to indicate this fact, this article is hereby marked "advertisement" in accordance with 18 USC section 1734.

Note

Supplementary data for this article are available at Cancer Immunology Research Online (http://cancerimmunolres.aacrjournals.org/).

Received April 15, 2022; revised August 1, 2022; accepted October 12, 2022; published first October 18, 2022.

References

1. Hanahan D, Coussens LM. Accessories to the crime: functions of cells recruited to the tumor microenvironment. Cancer Cell 2012;21:309–22.
2. Joyce JA, Fearon DT. T cell exclusion, immune privilege, and the tumor microenvironment. Science 2015;348:74–80.
3. Yano H, Andrews LP, Workman CJ, Vignali DAA. Intratumoral regulatory T cells: markers, subsets and their impact on anti-tumor immunity. Immunology 2019;157:232–47.
4. Dadey RE, Workman CJ, Vignali DAA. Regulatory T cells in the tumor microenvironment. Adv Exp Med Biol 2020;1273:105–34.
5. Buszko M, Shevach EM. Control of regulatory T cell homeostasis. Curr Opin Immunol 2020;67:18–26.
6. Brunkow ME, Jeffery EW, Hjerrild KA, Paeper B, Clark LB, Yasayko SA, et al. Disruption of a new forkhead/winged-helix protein, scurfin, results in the fatal lymphoproliferative disorder of the scurfy mouse. Nat Genet 2001;27:68–73.
7. Fontenot JD, Gavin MA, Rudensky AY. Foxp3 programs the development and function of CD4+CD25+ regulatory T cells. Nat Immunol 2003;4:330–6.
8. Maj T, Wang W, Crespo J, Zhang H, Wang W, Wei S, et al. Oxidative stress controls regulatory T cell apoptosis and suppressor activity and PD-L1-blockade resistance in tumor. Nat Immunol 2017;18:1332–41.
9. Curiel TJ, Coukos G, Zou L, Alvarez X, Cheng P, Mottram P, et al. Specific recruitment of regulatory T cells in ovarian carcinoma fosters immune privilege and predicts reduced survival. Nat Med 2004;10:942–9.
10. Saito T, Nishikawa H, Wada H, Nagano Y, Sugiyama D, Atarashi K, et al. Two FOXP3(+)CD4(+) T cell subpopulations distinctly control the prognosis of colorectal cancers. Nat Med 2016;22:679–84.
11. Turnis ME, Sawant DV, Szymczak-Workman AL, Andrews LP, Delgoffe GM, Yano H, et al. Interleukin-35 limits anti-tumor immunity. Immunity 2016;44:316–29.

12. Overacre-Delgoffe AE, Chikina M, Dadey RE, Yano H, Brunazzi EA, Shayan G, et al. Interferon-gamma drives Treg fragility to promote anti-tumor immunity. Cell 2017;169:1130–41.
13. Overacre-Delgoffe AE, Vignali DAA. Treg fragility: a prerequisite for effective antitumor immunity? Cancer Immunol Res 2018;6:882–7.
14. Sakaguchi S, Vignali DA, Rudensky AY, Niec RE, Waldmann H. The plasticity and stability of regulatory T cells. Nat Rev Immunol 2013;13:461–7.
15. Delgoffe GM, Woo SR, Turnis ME, Gravano DM, Guy C, Overacre AE, et al. Stability and function of regulatory T cells is maintained by a neuropilin-1-semaphorin-4a axis. Nature 2013;501:252–6.
16. Chuckran CA, Liu C, Bruno TC, Workman CJ, Vignali DA. Neuropilin-1: a checkpoint target with unique implications for cancer immunology and immunotherapy. J Immunother Cancer 2020;8:e000967.
17. Sarris M, Andersen KG, Randow F, Mayr L, Betz AG. Neuropilin-1 expression on regulatory T cells enhances their interactions with dendritic cells during antigen recognition. Immunity 2008;28:402–13.
18. Hansen W, Hutzler M, Abel S, Alter C, Stockmann C, Kliche S, et al. Neuropilin 1 deficiency on CD4+Foxp3+ regulatory T cells impairs mouse melanoma growth. J Exp Med 2012;209:2001–16.
19. Togashi Y, Shitara K, Nishikawa H. Regulatory T cells in cancer immunosuppression - implications for anticancer therapy. Nat Rev Clin Oncol 2019;16:356–71.
20. Parker BS, Rautela J, Hertzog PJ. Antitumour actions of interferons: implications for cancer therapy. Nat Rev Cancer 2016;16:131–44.
21. Fuchs SY. Hope and fear for interferon: the receptor-centric outlook on the future of interferon therapy. J Interferon Cytokine Res 2013;33:211–25.
22. Ortiz A, Gui J, Zahedi F, Yu P, Cho C, Bhattacharya S, et al. An interferon-driven oxysterol-based defense against tumor-derived extracellular vesicles. Cancer Cell 2019;35:33–45.
23. Huangfu WC, Qian J, Liu C, Liu J, Lokshin AE, Baker DP, et al. Inflammatory signaling compromises cell responses to interferon alpha. Oncogene 2012;31:161–72.
24. Bhattacharya S, HuangFu WC, Dong G, Qian J, Baker DP, Karar J, et al. Anti-tumorigenic effects of type 1 interferon are subdued by integrated stress responses. Oncogene 2013;32:4214–21.
25. Katlinski KV, Gui J, Katlinskaya YV, Ortiz A, Chakraborty R, Bhattacharya S, et al. Inactivation of interferon receptor promotes the establishment of immune privileged tumor microenvironment. Cancer Cell 2017;31:194–207.
26. Gui J, Zahedi F, Ortiz A, Cho C, Katlinski KV, Alicea-Torres K, et al. Activation of p38alpha stress-activated protein kinase drives the formation of the pre-metastatic niche in the lungs. Nat Cancer 2020;1:603–19.
27. Zhang H, Yu P, Tomar VS, Chen X, Atherton MJ, Lu Z, et al. Targeting PARP11 to avert immunosuppression and improve CAR T therapy in solid tumors. Nat Cancer 2022:808–20.
28. Lightcap ES, Yu P, Grossman S, Song K, Khattar M, Xega K, et al. A small-molecule SUMOylation inhibitor activates antitumor immune responses and potentiates immune therapies in preclinical models. Sci Transl Med 2021;13:eaba7791.
29. Bhattacharya S, Katlinski KV, Reichert M, Takano S, Brice A, Zhao B, et al. Triggering ubiquitination of IFNAR1 protects tissues from inflammatory injury. EMBO Mol Med 2014;6:384–97.
30. Katlinskaya YV, Katlinski KV, Yu Q, Ortiz A, Beiting DP, Brice A, et al. Suppression of type I interferon signaling overcomes oncogene-induced senescence and mediates melanoma development and progression. Cell Rep 2016;15:171–80.
31. Bhattacharya S, Qian J, Tzimas C, Baker DP, Koumenis C, Diehl JA, et al. Role of p38 protein kinase in the ligand-independent ubiquitination and down-regulation of the IFNAR1 chain of type I interferon receptor. J Biol Chem 2011;286:22069–76.
32. Ding X, Wang A, Ma X, Demarque M, Jin W, Xin H, et al. Protein SUMOylation is required for regulatory T cell expansion and function. Cell Rep 2016;16:1055–66.
33. van der Veeken J, Gonzalez AJ, Cho H, Arvey A, Hemmers S, Leslie CS, et al. Memory of inflammation in regulatory T cells. Cell 2016;166:977–90.
34. Binnewies M, Roberts EW, Kersten K, Chan V, Fearon DF, Merad M, et al. Understanding the tumor immune microenvironment (TIME) for effective therapy. Nat Med 2018;24:541–50.
35. Alicea-Torres K, Sanseviero E, Gui J, Chen J, Veglia F, Yu Q, et al. Immune suppressive activity of myeloid-derived suppressor cells in cancer requires inactivation of the type I interferon pathway. Nat Commun 2021;12:1717.
36. Cho C, Mukherjee R, Peck AR, Sun Y, McBrearty N, Katlinski KV, et al. Cancer-associated fibroblasts downregulate type I interferon receptor to stimulate intratumoral stromagenesis. Oncogene 2020;39:6129–37.
37. Zheng H, Qian J, Carbone CJ, Leu NA, Baker DP, Fuchs SY. Vascular endothelial growth factor-induced elimination of the type 1 interferon receptor is required for efficient angiogenesis. Blood 2011;118:4003–6.
38. Canovas B, Nebreda AR. Diversity and versatility of p38 kinase signalling in health and disease. Nat Rev Mol Cell Biol 2021;22:346–66.
39. Hatzioannou A, Banos A, Sakelaropoulos T, Fedonidis C, Vidali MS, Kohne M, et al. An intrinsic role of IL-33 in Treg cell-mediated tumor immunoevasion. Nat Immunol 2020;21:75–85.
40. Di Pilato M, Kim EY, Cadilha BL, Prussmann JN, Nasrallah MN, Seruggia D, et al. Targeting the CBM complex causes treg cells to prime tumours for immune checkpoint therapy. Nature 2019;570:112–6.
41. Gough DJ, Messina NL, Clarke CJ, Johnstone RW, Levy DE. Constitutive type I interferon modulates homeostatic balance through tonic signaling. Immunity 2012;36:166–74.
42. Metidji A, Rieder SA, Glass DD, Cremer I, Punkosdy GA, Shevach EM. IFN-alpha/beta receptor signaling promotes regulatory T cell development and function under stress conditions. J Immunol 2015;194:4265–76.
43. Srivastava S, Koch MA, Pepper M, Campbell DJ. Type I interferons directly inhibit regulatory T cells to allow optimal antiviral T cell responses during acute LCMV infection. J Exp Med 2014;211:961–74.
44. Gangaplara A, Martens C, Dahlstrom E, Metidji A, Gokhale AS, Glass DD, et al. Type I interferon signaling attenuates regulatory T cell function in viral infection and in the tumor microenvironment. PLoS Pathog 2018;14:e1006985.
45. Kawano Y, Zavidij O, Park J, Moschetta M, Kokubun K, Mouhieddine TH, et al. Blocking IFNAR1 inhibits multiple myeloma-driven Treg expansion and immunosuppression. J Clin Invest 2018;128:2487–99.